Coupling a CO_2 plasma with a carbon bed: the closer the better

Omar Biondo[1,*], Kaiyi Wang[2,*], Hao Zhang[2], Annemie Bogaerts[1]

[1]Research group PLASMANT, University of Antwerp, Department of Chemistry, Universiteitsplein 1, BE-2610 Wilrijk-Antwerp, Belgium.

[2]State Key Laboratory of Clean Energy Utilization, Zhejiang University, Hangzhou 310027, China

Corresponding authors:

[1]annemie.bogaerts@uantwerpen.be (Annemie Bogaerts)

[2]zhang_hao@zju.edu.cn (Hao Zhang)

*Shared first author

Abstract

We investigate plasma-based CO_2 conversion into CO, a valuable feedstock for producing hydrocarbons via Fischer-Tropsch synthesis. However, CO-rich outputs for industrial use are currently limited by recombination reactions and the presence of O_2 in the product stream. To address this, we place a carbon bed after the plasma to convert O_2 into additional CO, while exploiting the reverse Boudouard reaction to further enhance CO_2 conversion and CO enrichment. Previous studies have shown promising results, but reactor designs still need optimization, and the interaction between plasma and carbon bed remains unclear. In this study, we improve the coupling between the plasma and carbon bed, achieving outstanding performance, with CO_2 conversion exceeding 40% and energy cost below 2.8 eV/molecule (or 278 kJ/mol, corresponding to ca. 5 GJ per tonne CO or 1.4 kWh per kilogramme CO). This represents over a fourfold increase in conversion and nearly a fourfold reduction in energy cost compared to plasma experiments without carbon bed. Our detailed kinetic modeling reveals that the performance improvement is primarily due to the efficient removal of O_2, which is converted into CO_2, followed by the reverse Boudouard reaction, which enriches the CO output due to the high temperatures from close plasma contact. Thus, coupling a CO_2 plasma with a carbon bed boosts the industrial viability of CO_2 valorization, offering an attractive alternative to existing plasma-based CO_2 splitting technologies, which typically require an order of magnitude more energy for similar conversion levels.

Keywords: CO_2 conversion / plasma / biochar / carbon bed / reverse Boudouard reaction / CO enrichment

1. Introduction

CO_2 capture and utilization (CCU) is a strategic approach to mitigating climate change that has garnered increasing attention over the last decade. CO_2 utilization refers to the production of one or more economically valuable products from CO_2 conversion [1]. Among the various pathways, the production of CO through CO_2 splitting is particularly noteworthy, as CO serves as a primary feedstock for synthesizing liquid hydrocarbons via the Fisher-Tropsch process or for producing methanol and dimethyl ether through a two-step conversion process [2].

However, CO_2 splitting is inherently a highly endothermic reaction, requiring temperatures of at least 2000 K at atmospheric pressure [3]:

$$CO_2 \rightarrow CO + 1/2\ O_2, \text{ with } \Delta H_R^\circ = 283 \text{ kJ/mol (or 2.9 eV/molecule)} \quad (1)$$

At industrial level, heat for endothermic reactions is still largely provided by the combustion of fossil fuels, thus rendering CO_2 utilization drastically ineffective for decarbonization. Alternatively, endothermic processes can be electrified to recover their decarbonization potential and integrate them with renewable energy sources [4].

In this context, plasma is a valuable ally, as it has been demonstrated that its high-energy can activate highly endothermic reactions, such as CO_2 splitting, H_2O decomposition, and dry reforming of methane (DRM) [3,5,6]. Particularly, gas discharge plasmas offer the following advantages: 1) Chemical reactions can be driven through high-energy electrons and reactive species, overcoming the energy barriers of traditional thermal reactions, even without catalysts [5,6]; 2) They are generated by electricity, and can be quickly switched on/off, so they can be coupled with intermittent renewable energy generation, making them suitable for miniaturized and distributed applications and for electrification of chemical processes [7,8].

Various gas discharge plasmas have been employed for CO_2 conversion [3], including dielectric barrier discharges (DBD) [9,10], nanosecond repetitively pulsed (NRP) discharges [11–13], and so-called “warm” plasmas, such as gliding arc (GA) discharges [14,15] and microwave (MW) discharges [16–21], offering promising results. DBD can typically achieve relatively high CO_2 conversions (up to 90%) due to the presence of high-energy electrons (e.g., > 3 eV). However, its energy efficiency remains relatively low (< ~10%) [3], and its processing capacity is limited, generally handling only 10-100 mL/min, which hinders its scalability for industrial applications. On the other hand, both MW and GA plasmas offer reasonable CO_2 conversion (e.g., 20%) and improved energy efficiency (e.g., 30%), since they can theoretically utilize up to 90% of the electron energy for vibrational excitation, enabling CO_2 decomposition via the efficient "ladder-climbing" mechanism [22–24]. However, this vibrational dissociation pathway is not important when operating at atmospheric pressure, because of efficient vibrational-translational relaxation, depopulating the vibrational levels and resulting in gas heating (hence the name “warm” plasma). Therefore, in practice CO_2 decomposition in these warm plasmas, when operating at/near atmospheric pressure, mainly occurs by thermal chemistry. Thus, the highest energy efficiency of CO_2 conversion for MW plasmas is typically reported under low-pressure conditions (e.g., 40-130 mbar [17,25–27]), whereas at atmospheric pressure, high energy efficiency is only achieved together with low CO_2 conversion (ca. 10%) [28,29], or in particular configurations, *e.g.*, with quenching nozzles [20,30,31]. Therefore, at the status of development, energy-efficient CO_2 conversion in MW plasmas requires low-pressure operations, which increases the system complexity and energy cost. In addition, MW setups generally involve higher capital costs compared to other plasma technologies, such as GA discharges [32,33]. Hence, considering that MW and GA discharges have similar performance under equivalent experimental conditions (such as pressure and power) [34], the latter stand out due to their greater simplicity and cost reduction [32,33].

One of the main factors limiting the energy efficiency of warm plasmas is the recombination reactions between CO and O/O_2, which regenerate CO_2 and thus reduce the overall conversion [35]. A viable approach to overcoming this limitation is by quenching (i.e., fast cooling of the product gas, to avoid recombination) [30,31,36], or by the introduction of reducing agents, such as metal reductants [37,38], carbon materials [39–41], methane [42,43], or hydrogen [42,44], which remove oxygen from the products, thereby also suppressing CO_2 recombination reactions [38,44]. The oxygen removal not only enhances the CO_2 conversion but also reduces product separation costs in subsequent applications [7].

Among various reducing agents, carbon materials, particularly biochar, stand out due to their well-established preparation process, ready availability from renewable biomass, and highly porous structure with high reactivity, making them one of the best choices for improving sustainable CO_2 conversion [45,46]. However, their use presents challenges, notably their purity and solid-state nature. Purity affects the buildup of ash during gasification, with severity depending on the origin of the biochar. Excessive ash can hinder the process, while small amounts containing specific minerals, such as potassium [47], can enhance biochar reactivity during CO_2 gasification. In fact, alkali and alkaline earth metals are known catalysts for biochar gasification, whereas silicon and aluminum have an inhibiting effect [48]. The presence of SiO_2 and Al_2O_3 in biochar reduces its reactivity by forming inactive complex silicates with elements such as K, Na, Ca, Mg, and Fe [48]. This means that biochar reactivity is highly dependent on its material properties, denoting it cannot be treated as a uniform material but rather as a diverse and heterogeneous class of materials.

Another challenge of using biochar as a reducing agent stems from its solid-state nature, which limits the interaction between the gas and the biochar. To optimize gas residence time and maximize contact between the gas and the active sites of biochar, careful bed design is required.

The viability of biochar gasification with CO_2 is demonstrated by the number of works published in the last decades [49]. However, despite extensive research, many questions remain unresolved. These include understanding the relationship between biochar structure and gasification reactivity, isolating the effects of individual parameters within a complex web of interrelated factors, and exploring the use of catalysis to improve conversion while avoiding catalyst deactivation [49].

Temperature plays a crucial role in the gasification of biochar with CO_2 due to the high endothermicity of the process. This involves the splitting of inert CO_2 through dissociative chemisorption and, subsequently, the weakening of the local structure and rearrangement of the carbon surface to desorb CO [50]. This reaction, known as reverse Boudouard reaction (RBR), requires temperatures exceeding 1000 K [48]:

$$C(s) + CO_2(g) \rightleftharpoons 2\,CO(g), \text{ with } \Delta H_R^\circ = 172 \text{ kJ/mol (or 1.8 eV/molecule)} \quad (2)$$

Various heat sources have been explored to enhance the RBR rate during gasification, including conventional convective heating [48,51], solar-driven gasification [52–54], and microwave-driven CO_2 gasification [51,55–57]. Notably, MW heating has demonstrated a 60–70% reduction in the activation energy for CO_2 gasification and achieved energy efficiencies of 45% at the laboratory scale [58]. However, substantial further research is needed to scale this technology for industrial applications [49].

Recent studies have shown significant promise in plasma-driven RBR with solid carbon [39–41,59–62]. Plasma not only provides the heat required to activate biochar reactivity but also generates a reactive gas mixture that can lower energy barriers for surface reactions or even introduce new reaction pathways. In plasma-based CO_2 conversion, this involves producing O atoms and O_2, following reaction in Eq. (1), resulting in a combination of CO_2 and O_2 gasification when biochar is used [41]. Typically, biochar is introduced in a plasma reactor downstream of the discharge zone, either as a fluidized or fixed bed [40]. This setup allows for better utilization of the waste heat from the plasma to convert unreacted CO_2 molecules through RBR (Eq. 2). In addition, biochar reacts with O_2 (or O atoms) to produce additional CO, further improving CO_2 conversion by removing one of the splitting products, suppressing recombination reactions, and enriching the product stream of CO This is highly advantageous for industrial application, as separation of O_2 from CO remains a significant challenge [63] and a critical factor in the overall process cost [7]. Notably, achieving an O_2-free exhaust gas (i.e., ideally pure CO) is essential for directly utilizing the output of CO_2 splitting in industrial processes, such as the Fischer-Tropsch synthesis.

One of the earliest applications of plasma-driven RBR was reported by Uhm *et al*. [59] where coal powder was introduced downstream of a CO_2 MW discharge. The authors achieved an optimal CO_2 conversion of 40% under their highest specific energy input (SEI) conditions, corresponding to 24 kJ/L (5.99 eV/molecule) with a high power input of 4 kW and a low flow rate of 10 L/min. Subsequently, Liu *et al*. [60] employed an atmospheric pressure thermal plasma (TP) torch operating in a mixture of Ar and CO_2 to react with coke particles ranging from 5 to 8 mm in diameter. Their highest CO_2 conversion of 95% was achieved with a power input of 16 kW and a near 1:1 mixture of Ar and CO_2 (25 L/min and 26 L/min, respectively). When the CO_2 fraction was increased to a maximum ratio of 1:1.4 (Ar:CO_2) at a fixed power of 14 kW, the conversion decreased to 68%. However, this adjustment resulted in an improved energy cost (EC) of 0.34 MJ/mol CO, since effective conversion (which accounts for the fraction of CO_2 at the inlet) increased. Further research by Li *et al*. [61] extended the work of Liu *et al*. [60] by investigating the impact of introducing CO_2 into the afterglow of a TP discharge rather than using it as one of the discharge gases. They also employed optical emission spectroscopy (OES) to analyze the species present in the afterglow. When CO_2 was introduced as a discharge gas, the inlet stream was diluted with Ar, similar to the approach of Liu *et al*. [60], and C_2 Swan band emissions were observed in the afterglow, showing that significant dissociation had occurred. Instead, injecting CO_2 into the afterglow of an Ar/N_2 discharge yielded no detectable C_2 Swan band emissions, indicating minimal or no CO_2 dissociation. Swapping afterglow for plasma injection increased CO_2 conversion from 35% to 70%. The authors attributed this enhancement to the combined effects of plasma-based CO_2 dissociation and RBR occurring in the carbon bed.. Most recently, Wu *et al.* [62] combined an atmospheric pressure MW plasma with a carbon

bed, using Ar and CO_2 as input gases. The authors examined the influence of Ar dilution on system performance, finding a nearly linear increase in absolute CO_2 conversion with rising Ar fractions. The energy efficiency peaked at Ar fractions of 30–40%, but decreased at higher concentrations due to the disproportionate allocation of energy to Ar ionization rather than CO_2 dissociation. Finally, the authors compared biochar derived from two sources, namely coconut shell and bamboo. The smaller coconut shell char yielded the best results, with an optimal absolute CO_2 conversion of 75% and a corresponding energy efficiency of 30%. However, when accounting for the proportion of CO_2 relative to the total feed gas mixture, the effective CO_2 conversion was determined to be 60%.

This works have proven the effectiveness of combining a carbon bed with a TP, with the latter providing strong heat fluxes needed to activate the highly endothermic RBR. Despite this, what appears to be an advantage for the carbon bed reactivity becomes a significant drawback for the lifetime of the reactor, particularly for the electrodes, which are highly susceptible to corrosion due to the high temperatures and resulting exposure to a strongly oxidizing environment. To mitigate this effect, argon is added to the CO_2, but this significantly increases the process cost, both due to the price of argon and the additional expense of separating the products from argon. This limitation can be circumvented by employing electrodeless configurations, such as in the case of MW plasmas. However, this setup has been studied very little to date as shown Table 1, and there is no guarantee that argon is not still used, as in the case of Wu *et al*. [62], who do not specify whether it was added to protect the reactor or for other reasons.

Alternatively, warm plasmas can be employed without the need to introduce an inert gas, thanks to the milder discharge conditions, which result in reduced reactor degradation. Huang *et al*. [39] demonstrated the first implementation of a post-plasma carbon bed with a CO_2 gliding arc plasmatron (GAP). In the presence of carbon, the peak CO_2 conversion improved from approximately 7% to 21%, though at the expense of energy efficiency, which dropped from 36% to 24%. The observed reduction in energy efficiency occurs because the optimum flow rate for conversion with biochar is lower than in the empty reactor case. Nevertheless, their study proves that the carbon bed can improve CO_2 conversion even at average temperatures lower than those observed in previously studied TPs. Subsequently, Zhang *et al*. [40] studied the effects of solid carbon characteristics and fluidization on the CO_2 conversion in a similar GAP setup, revealing that materials with higher carbon content yielded better conversion, while fluidized beds showed lower conversion, due to a combination of a lower measured gas temperature and a higher recombination rate of the produced CO and O_2 due to the longer pathway before reacting with the biochar. The authors also conducted thermal RBR experiments, wherein heat was supplied to the gas externally without plasma. These experiments revealed that the maximum CO_2 conversion achievable through thermal RBR is approximately 5.3% at 1273 K, significantly lower than the 27.1% and 41.5% obtained with plasma in [40] and in this paper, respectively. The results from these thermal RBR experiments were used to calibrate the kinetic model employed in this study, as detailed later in Section 3.2. At the same time, Girard-Sahun *et al*. [41] investigated the addition of solid carbon to another GAP reactor, reporting enhanced CO_2 conversion and energy efficiency by almost a factor two, a reduction in energy cost by almost a factor two, and even three times higher CO yield, while nearly completely removing O_2. Furthermore, they linked their experimental results with kinetic modeling, showing how the carbon bed increases the CO_2 conversion, by removing oxygen, although deactivation occurred over time due to surface saturation with oxygen complexes. More recently, O'Modhrain *et al*. [64] further improved the performance of this GAP reactor by switching from AC to DC to increase the effluent gas temperature and by optimizing the carbon bed design, specifically evaluating the effects of bed length and additional insulation. They tested three different carbon beds, using the same type of activated carbon at two distinct SEI values. With the longest bed, they achieved a maximum CO_2 conversion of 41%, a minimum EC of 4.25 eV/molecule, and a peak energy efficiency of 51%.

Overall, these studies indicate that placing a carbon bed downstream a CO_2 plasma can significantly enhance the CO_2 conversion and, as a result, the energy efficiency. The latter metric is however difficult to determine when the conversion process involves solid reactants that are highly inhomogeneous, like carbon from biomass pyrolysis. First of all, it is important to determine which reactions are potentially contributing to the conversion process, and specifically how much CO_2 is dissociated in the gas phase or at the carbon surface through the RBR. Additionally, partial oxidation reactions, converting O/O_2 into further CO, are also crucial for calculating energy efficiency. In order to correctly calculate the energy efficiency, the contribution of each reaction channel must be known; however, this can only be estimated through detailed kinetic modelling [41] or by making key assumptions on the reaction pathways. But even if we know the contribution of

each reaction, energy efficiency can only be calculated by knowing the enthalpy associated with each reaction. This is even more difficult to estimate, because the energy associated with each carbon active site depends on numerous factors, such as structure, degree of oxidation, presence of impurities (*e.g.*, H_2) [50,65,66]. Therefore, in order to compare the performance of CO_2 splitting with and without a carbon bed, we believe EC is a more appropriate performance metric than energy efficiency, as it does not require detailed information about the enthalpy of the reactions involved. EC as a function of CO_2 conversion for plasmas with and without carbon bed, reported in literature and in this work, is compared in Figure 1.

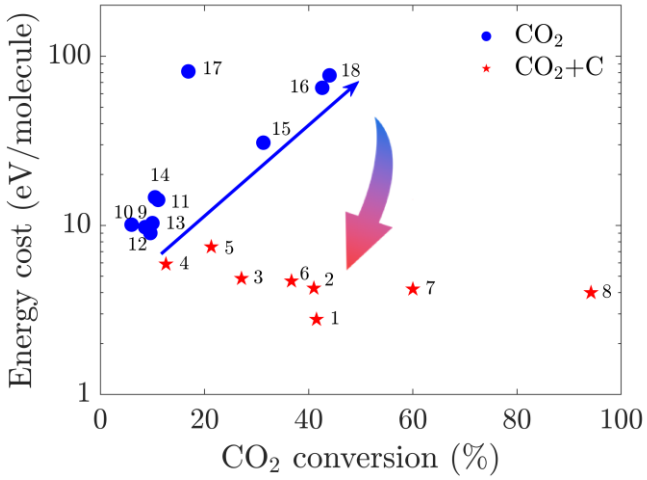

Figure 1. Energy cost vs CO_2 conversion for plasma-based CO_2 conversion without (blue spheres) and with (red stars) carbon materials. The numbers correspond to the first column in Table 1, which provides more information on the plasma type, exact values of the performance metrics, operating conditions, and the corresponding references.

"Table 1. Comparison of the performance of CO_2 conversion among different plasmas. Each row corresponds to a point in Figure 1, labelled according to the first column. Experiments with a carbon bed are denoted according to the plasma type, followed by "+C". If argon is introduced in the feed gas, its flow rate is specified along with that of CO_2.

Label Fig.1	Plasma type	CO_2 conversion (%)	Energy cost (eV/molecule)	CO_2 flow rate (L/min)	Power (W)	Reference
1	GAP+C	41.5	2.8	5	412	This work
2	GAP+C	41	4.25	10	1133	[64]
3	GAP+C	27.1	4.9	5	470	[40]
4	GAP+C	12.6	3.9	10	533	[41]
5	GAP+C	21.3	7.5	4	454	[39]
6	MW+C	36.7	4.7	10	1600	[62]
7	MW+C	60	4.2	4.8+Ar(1.2 L/min)	1800	[59]
8	TP+C	94.2	4	23+Ar (25 L/min)	14000	[60]
9	GAP	10	10.3	7	519	[40]
10	GA	6	10.1	10	400	[67]
11	GA	11.1	14.2	3	339	[68]
12	GA	9.6	9.0	6.5	404	[15]
13	GAP	8.6	9.8	10	604	[14]
14	MW	10.5	14.7	16	1675	[16]
15	MW	31.3	30.8	5	3500	[18]
16	MW	42.6	65.1	1.2	120	[19]

17	DBD	16.9	81.4	4.37×10^{-2}	60	[10]
18	DBD	44	77.1	5×10^{-2}	30	[9]

The comparison highlights that, in plasma-based pure CO_2 splitting (without carbon bed), a high conversion is associated with high EC. Interestingly, the opposite trend is observed when carbon materials are added, significantly reducing EC, while simultaneously increasing conversion. Osorio-Tejada *et al*. [69] compared EC of producing one tonne of CO using the plasma-driven RBR method from Girard-Sahun *et al*. [41] with CO_2 electrolysis and other conventional methods for CO_2 splitting. They found that the use of a carbon bed resulted in a 43% reduction in EC. This reduction is even more remarkable when considering that our best results achieve a cost of approximately 5 GJ per tonne CO or 1.4 kWh per kilogramme CO, whereas Girard-Sahun *et al*. [41] obtained a minimum EC of 19 GJ per tonne CO or 5.32kWh per kilogramme CO. The plasma-driven RBR method not only reduces EC, but also the environmental impact of producing CO. A recent lifecycle analysis, together with a detailed calculation of Green Chemistry and circularity metrics, performed by Escribà-Gelonch *et al*. [70], demonstrated that plasma-driven RBR outperforms both electrolysis and conventional partial combustion of fossil fuels in 7 out of 10 environmental impact categories. Moreover, plasma technology achieves 40% energy savings, 10% higher material circularity indicator**,** 10–30% higher Green Chemistry metrics, and 7% lower global warming potential emissions compared to electrolysis. This is a result of lower water consumption and contamination, reliance on fossil fuels, electricity demand, waste generation, and material requirements, along with improved recycling loops. This makes the coupling of CO_2 plasma with a carbon bed very promising to meet industrial requirements for high, oxygen-free CO outputs with lower EC. Nevertheless, challenges remain in managing unwanted reactions and maintaining performance over time [41].

As far as we know, the only implementation of plasma-based RBR at the pilot scale is from D-CRBN [71], spinoff company of our research group PLASMANT. Their pilot-scale plasma prototype, termed the multi-reactor gliding arc plasmatron and described in the work of O'Modhrain *et al*. [33] for pure CO_2 splitting, features a unified reactor body with five approximately 1 kW reactor nodes, totaling 5 kW. Experiments in this setup with post-plasma carbon bed showed significant improvements compared to plasma-only. However, this total power remains far from the industrial-scale plasma reactors envisioned for CO_2 conversion, which would require 100 kW to 1 MW of power [72].

Upscaling has proven to be effectively achieved by placing multiple reactors in parallel. However, care must be taken for more complex heat management, faster degradation, and thus shorter lifespans at much higher power. For CO_2 splitting, it has been demonstrated that lab-scale performance can be retained in pilot-scale reactors [33].

Building on this precedent, our work focuses on advancing the state of the art at lab scale, with the hypothesis that these improvements can be transferred to the pilot scale, as seen in the case of pure CO_2 splitting. Therefore, we expand upon the lab-scale studies of Zhang *et al*. [40] and Girard-Sahun *et al*. [41], testing various designs for the coupling of plasma and carbon beds and using a detailed kinetic model to interpret the experimental results. The designs tested here are compared with that in [40], with the main variable being the distance between the plasma and the carbon bed. The optimized configuration in this work achieves a CO_2 conversion of 41.5% and an EC of 2.8 eV/molecule, while maintaining a high processing capacity of 5 L/min CO_2, as summarized in Table 1. The model from [41] is adapted to investigate the performance under the specific experimental parameters of this study. The kinetics are first calibrated with thermal gasification experiments, where heat is provided externally in a furnace rather than from the plasma. This allows for the gas temperature within the carbon bed to be homogeneous and controlled, as well as for the composition of the incoming gas to be known, which consists of a mixture of CO_2 and decomposition products when plasma is present before the carbon bed. Therefore, these experiments serve as the ideal benchmark for a kinetic model. After calibrating the kinetics, parameter sweeps are conducted to determine how the performance changes with various conditions. Finally, the model outcomes are linked to the experimental results.

The combination of experiments and modeling allows us to explain why certain reactor modifications improve process performance and how these improvements can be transferred to other reactors, especially with a view toward scaling up. Specifically, in this study, we observe that reducing the distance between the plasma and the carbon bed enhances

performance, but this is not due to the quenching of recombination reactions, but rather because of the increased heat available for the carbon surface to convert CO_2 into CO through the RBR. Without these insights from the model, one might mistakenly believe that performance is solely determined by the complete removal of O/O_2 from the reactive mixture and its conversion into CO. As we will discuss later in the results and discussion section, the interpretation of the experimental results can significantly impact the guidelines for future development.

2. Experimental section

2.1. Experimental setup and methods

The schematics of the GAP reactors with different plasma-carbon bed configurations are shown in Fig. 2. The GAP reactor features a cylindrical inner anode and a convergent, nozzle-shaped outer cathode (grounded), both constructed from stainless steel. The anode is powered by a 10 kV DC power supply (TLP2040, Teslaman), operated in constant-voltage mode during the experiments. The resulting power input ranges between 300 and 500 W, depending on the gas flow rate. To stabilize and limit the discharge current, a 40 kΩ resistor is connected in series within the circuit. The feed gas, CO_2 (99.99% purity), is introduced through a tangential inlet at the base of the cathode, creating a swirling flow inside the reactor for plasma formation and stabilization. The flow rate is precisely controlled by a mass flow controller (MFC, YJ-700C). The arc is ignited at the narrowest gap (2 mm) between the electrodes and is subsequently propelled downstream, rotating rapidly around the anode. The resulting plasma extends from the convergent nozzle exit, forming a large, 3D, torch-like plasmatron beyond the electrode region. A quartz cover with a gas exit at the top encloses the plasmatron reaction zone, while a plug of quartz glass wool is positioned at the exit of the quartz cover to prevent biochar particles from escaping. Inside the quartz tube, a quartz screen mesh (1 mm diameter openings) holds the carbon particles in place within the carbon bed, preventing them from falling into the discharge zone, which could disrupt plasma stability. The screen mesh showed no visible degradation, even after dozens of experiments, including those in Reactor B, where the plasma distance is reduced to 1 mm. In addition, no discharge between the anode and the carbon bed was observed during testing. For each experiment, 1.2 g of biochar is loaded to the fixed carbon bed. During the experiments, the plasma primarily interacts with the upper layer of the carbon bed, which is gradually consumed, exposing the lower layers until all carbon particles are fully reacted. The experiments continue until the biochar is completely consumed, as indicated by the product concentrations and CO_2 conversion returning to the steady-state values observed in the absence of carbon, i.e., with an empty bed. Complete biochar consumption occurs between 2 or 3 minutes of reaction, depending on the experimental conditions. Photographs in Figure 2, showing the carbon bed during the reaction, confirm that the space between the biochar particles is sufficient to prevent gas flow clogging and significant pressure buildup upstream of the carbon bed. Each experimental condition is repeated three times, and the average results, along with the corresponding standard deviations, are presented in Section 4.1.

Three different GAP reactor configurations are compared in this study. Reactor A, which was studied earlier in our group [40], and Reactors B and C, which are new configurations developed within this work. All three configurations share the same electrodes and quartz tubes. However, the distance between the plasma and the screen mesh for holding biochar is reduced from 10 to 1 mm in Reactor B, whereas the screen mesh is removed in Reactor C. In fact, the latter is rotated by 180° and, consequently, a screen mesh is no longer needed to prevent carbon particles from falling in the discharge zone.

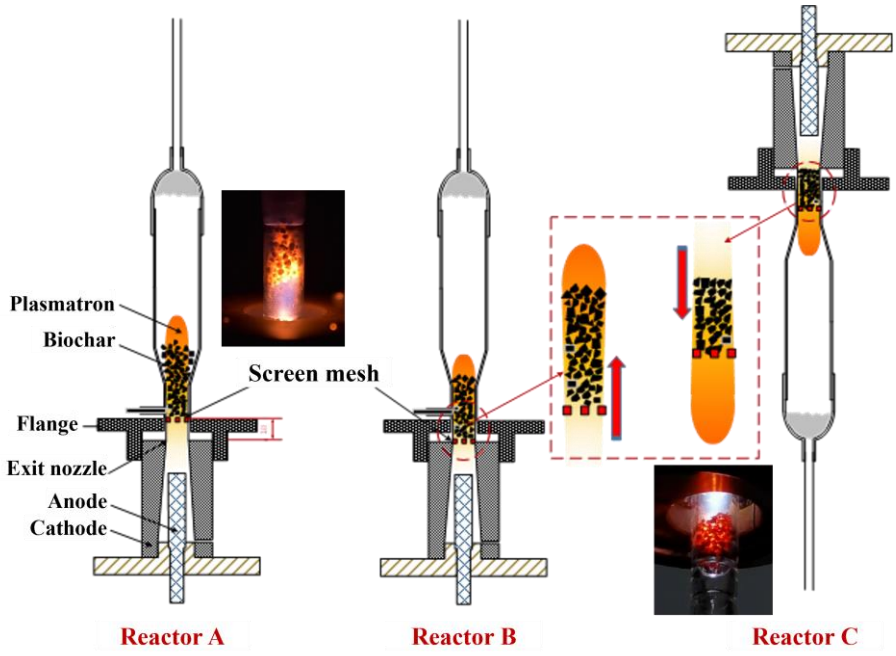

Figure 2. Schematics of Reactor A, B and C with different plasma – fixed carbon bed configurations.

CO_2 and CO concentrations are monitored in real time by an online gas analyzer (UE-50, ONUEE), equipped with non-dispersive infrared (NDIR) sensors, with a sampling interval of 2 s. From these measurements, CO_2 conversion (X_{CO_2}) is defined as:

$$X_{CO_2}(\%) = \frac{Q_{in}(\text{mol/min}) \times C_{CO_2,in}(\%) - Q_{out}(\text{mol/min}) \times C_{CO_2,out}(\%)}{Q_{in}(\text{mol/min}) \times C_{CO_2,in}(\%)} \quad (3)$$

where Q_{in} and Q_{out} are the inlet and outlet total gas flow rates, respectively, and $C_{CO_2,in}$ and $C_{CO_2,out}$ are the CO_2 concentrations in the inlet and outlet gas, respectively. Conversion is calculated taking the change in molar flow rate after the reaction into account [73]. In effect, Q_{out} is generally not equal to Q_{in}; therefore, Q_{out} is calculated from the oxygen balance, following the procedure of Zhang *et al*. [40].

The specific energy input (SEI) is defined as:

$$\text{SEI(kJ/mol)} = \frac{\text{Discharge power(W)} \times 60(\text{s/min}) \times V_m(\text{L/mol})}{Q_{in}(\text{L/min}) \times 1000(\text{J/kJ})} \quad (4)$$

where V_m is the molar volume of gas (22.41 L/mol at 273 K and 1 atm).

EC is defined as the amount of energy consumed per mole of CO_2 converted, as follows:

$$\text{EC (eV/molecule)} = \frac{\text{Discharge power(W)} \times 60(\text{s/min})}{X_{CO_2} \times Q_{in}(\text{mol/min}) \times 1.60\times10^{-19}(\text{J/eV}) \times N_A(\text{molecule/mol})} \quad (5)$$

where N_A is Avogadro's constant (6.022×10^{23} molecule/mol). The discharge power is calculated by integrating the product of voltage between both electrodes and discharge current over time:

$$\text{Discharge power(W)} = \frac{1}{\Delta T}\int U(V)\cdot I(A)\, dt \quad (6)$$

It should be noted that due to the continuous consumption of biochar in the carbon bed, the product com position could not reach a stable state (see Figure 8(d) below). Therefore, the conversion and EC presented in this paper represent the maximum values obtained in each experiment.

2.2. Biochar characterization

The biochar used in this study is prepared from walnut shells (Zhengjie Environmental Protection Technology Co., Ltd.) through pyrolysis in a tube furnace (SKF-2-13, LTYQ, China). Initially, the walnut shells are crushed to a particle size of 2-3 mm. This size facilitates the production of biochar particles with the desired size after pyrolysis. Before pyrolysis, the shells are thoroughly cleaned, and dried at 353 K for 12 hours. The dried shells are then heated in a nitrogen atmosphere (flow rate: 150 mL/min) at a rate of 10 K/min up to 773 K, where the temperature is maintained for 3 hours to ensure complete pyrolysis. Afterward, the biochar is naturally cooled to room temperature under the same nitrogen atmosphere. The resulting biochar is sieved to obtain particles with a diameter of 1-2 mm, which is sufficiently small to pack inside the carbon bed and sufficiently large to not pass through the screen mesh. Moreover, we chose the smallest possible size to maximize the surface area for better contact with the plasma. This preparation protocol was shown to provide the best performing biochar among all carbonaceous materials tested in our previous work [40]. The specific surface area and pore structure of the biochar are characterized using an automatic surface area and pore size analyzer (Quantachrome Autosorb IQ3). Nitrogen adsorption-desorption isotherms are measured at 77.3 K following degassing at 473 K. The specific surface area is determined using the Brunauer-Emmett-Teller (BET) adsorption model. Proximate analysis is performed with an automatic proximate analyzer (5E-MAG6700), while ultimate analysis is conducted using an elemental analyzer (5E-CHN2000). Proximate analysis is performed with an automatic proximate analyzer (5E-MAG6700), with water determined in air at 378 K, ash determined in air at 1088 K, and volatile matter determined in nitrogen at 1173 K. Ultimate analysis is conducted using an elemental analyzer (5E-CHN2000), with the combustion tube at 1423 K and the reduction tube at 1123 K. The results of these characterizations are presented in Tables 2 and 3.

Table 2. Specific surface area and pore structure of the walnut shell biochar.

Surface area (m^2/g)	Micropore area (m^2/g)	Total pore volume (cm^3/g)	Average pore diameter (nm)
28.6	33.5	0.02	35.1

Table 3. Proximate and ultimate analyses of the walnut shell biochar.

Proximate analysis (wt %)				Ultimate analysis (wt %)[a]				
Water	**Ash**	**Volatiles**	**Fixed carbon**	**C**	**H**	**O**	**N**	**S**
3.26	1.66	10.38	84.7	86.04	2.69	6.17	0.18	0.06

[a]Note that the elemental weight percentages sum to 95.16%. Based on the literature, we hypothesize that the remaining percentage could be attributed to trace metal elements and silicon [74,75].

2.3. Thermal oxidation experiment

Thermal oxidation experiments without plasma are conducted in a tubular furnace for model calibration, as shown later in section 3.2. 8 g of biochar, prepared as described in section 2.2, are placed in a quartz tube with an inner diameter of 16 mm. A nitrogen-oxygen mixed gas (N_2 : O_2 = 95 : 5) with a total flow rate of 4 L/min is introduced into the system. The sample is heated from 300 K to 1200 K at a rate of 12 K/min. The resulting products, including CO, CO_2, CH_4, H_2, and O_2, are detected online using a flue gas analyzer (GASBOARD-3100, Wuhan Cubic Optoelectronic Co., Ltd.), equipped with a thermal conductivity detector (TCD) for H_2, an electrochemical sensor for O_2, and a NDIR sensor for the other products.

3. Modeling section

3.1 Kinetic model

The kinetic model used in this study is zero-dimensional (0-D), also referred to as "global", as all quantities are assumed to be homogeneous within the computational volume [76]. Therefore, it is a spatially-averaged model in which the continuity equation is solved for five gas-phase species, namely CO_2, CO, O_2, O, and C, and two surface species, C(s) and C(s)-O. The latter species represent an active carbon site, and an oxygen atom chemisorbed at an active carbon site,

respectively [41,77]. Spatial variations due to transport phenomena are not directly considered but are instead approximated by assuming a plug-flow reactor configuration. In this framework, chemical species move together with an infinitesimally small volume of gas along the reactor axis [76], except for the surface species, C(s) and C(s)−O, which are treated as solid-state species. As such, they do not move with the gas and do not contribute to defining the gas density.

When the plasma reactor is treated as a plug-flow reactor, temporal variations in gas-related quantities correspond to variations as a function of the gas residence time in the reactor, or equivalently, as a function of the distance within the reactor. Variations in temperature and molar flow rate due to chemical reactions, such as expansion or molar flow rate increase from, e.g., CO_2 splitting or CO desorption from the carbon surface after RBR, are accounted for by adjusting the calculated species densities to ensure constant pressure throughout the simulation and by updating the gas velocity to maintain constant mass flux.

In this model, no energy balance equation for heavy particles is solved as the gas temperature is an input parameter rather than calculated self-consistently based on input power, reaction enthalpy, and thermodynamic properties of the mixture. The plasma is thus approximated as a heat source, and the contributions of electrons are neglected. Introducing an energy balance equation with sufficient accuracy in the presence of solid carbon remains unfeasible at the current stage of development. This limitation arises due to the high energetic inhomogeneity of carbon surface reactions, as pointed out by Calo and Perkins for RBR [78], making it highly challenging to assign unambiguously an enthalpy to each elementary surface reaction accounted for by the model. To overcome this, both *in-situ* diagnostics, capable of determining the composition and energetics of surface active sites [79,80], and DFT calculations, providing accurate rate coefficients for the reactivity of different active sites, e.g., [81], are crucial. Only with this information can detailed kinetic modelling be validated across a broader range of materials and assessed for solving an energy balance equation. However, this is feasible only if solid-gas heat transfer can be reasonably approximated, otherwise detailed kinetic modelling must be coupled with multi-dimensional simulations, resulting in a significant increase in computational cost.

The 0-D model is solved using ZDPlasKin [82] and is based on previous work from Girard-Sahun *et al*. [41], thus we refer to that article for more details regarding the kinetic model and the selection of the reaction set. To our knowledge, only two models for carbon gasification are available in the literature: our model and that of Girard-Sahun *et al*. [41]. Both combine a reverse Boudouard reaction kinetic scheme from Yang and Yang [83] with a carbon ablation model from Prata *et al*. [84]. While several carbon ablation models exist in the literature, Girard-Sahun *et al*. tested various approaches and concluded that the model by Prata *et al*. [84], which we employ, is the most complete and suitable for studying carbon gasification.

3.2 Model calibration

Earlier in the Introduction, we noted that carbon materials are highly heterogeneous in terms of structure and composition, resulting in surface active sites with varying concentration, energy and reactivity toward gas-phase species. Due to this heterogeneity, it is not feasible to develop a kinetic model that applies universally to all carbon materials, necessitating calibration of the model for the specific material being studied.

The kinetic model of [41] was originally developed and tuned for carbon fibers, using thermal gasification experiments conducted under controlled temperature and low pressure [85]. Insights from these validation steps were applied to explain trends observed in the combination of a CO_2 GAP with a charcoal bed, based on the assumption that different materials, such as fibers and charcoal, would not significantly alter the reaction mechanism. In the present study, the carbon materials and experimental conditions differ again. For instance, carbon fibers used in the model tuning have high carbon purity (>90%) [86,87] and low surface area (<10 m^2/g) [41,88], while biochars typically have lower purity (<90%) [89] (see also Table 2) and higher surface area (>10 m^2/g) [90] (see also Table 2). Given these differences, using the existing model and insights from [41] to interpret the results, maintaining the same assumption regarding reaction mechanisms, might not be very accurate.

Therefore, since we could perform thermal gasification experiments under conditions similar to those used in the plasma experiments, using the same materials and pressures, we choose to calibrate the CO_2 gasification (thermal Boudouard) kinetics for the new material using data from Zhang *et al*. [40]. We refer to this process as *calibration* rather than *validation,* because it adjusts the model specifically for the carbon material under study. For each new material, this calibration process must be repeated to ensure that the model accurately reflects the specific properties of the material. Thus, the model is only validated for the particular carbon material it has been calibrated for, and cannot be generalized without further calibration for different materials. Additionally, we conducted new thermal experiments to calibrate the oxidation (O_2 gasification) kinetics under these new experimental conditions. These new experiments are detailed in Section 2.3 above.

In the calibration process, a new parameter (*b*) is introduced to adjust the adsorption and collision-induced desorption rate coefficients, *k*, as follows:

$$k' = b*k \tag{5}$$

where *k'* is the adjusted rate coefficient. The rate coefficients for spontaneous desorption and surface oxidation remain unchanged. The tuning of the parameter *b* is demonstrated using CO_2 and O_2 gasification experiments, as shown in Figure 3 and 4, respectively. Both the gas temperature, which is fixed in each simulation, and the initial gas composition are given in the figure captions.

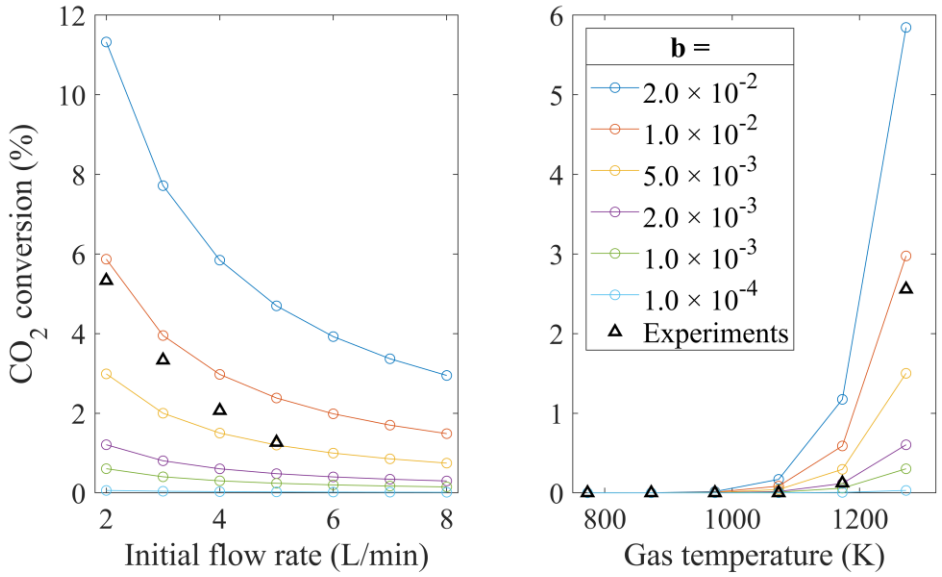

Figure 3. CO_2 gasification experiments (without plasma), (left) as a function of flow rate (constant temperature of 1273 K and pure CO_2 feed gas) and (right) as a function of gas temperature (constant flow rate of 4 L/min), published in [40], compared with modeling results (solid lines) varying the *b* parameter.

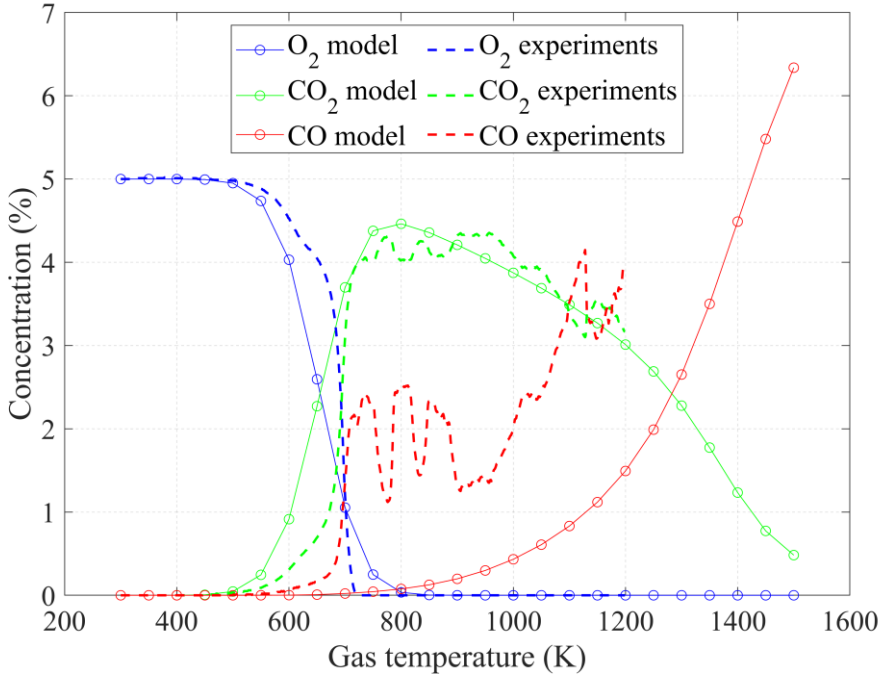

Figure 4. Species concentration as a function of gas temperature for the thermal oxidation experiment (dashed lines) and the model (solid lines) for b = 1 x 10^{-2}, taken from the calibration with the thermal Boudouard experiments of Figure 3. Each point corresponds to an individual simulation where the initial gas composition is O_2:N_2 5:95, while the gas temperature is fixed and specified on the x-axis.

These figures indicate that both CO_2 and O_2 gasification experiments are well reproduced by the model when b = 1 x 10^{-2}, suggesting that the reactivity of the carbon bed in this study is lower compared to the conditions modeled in [41]. This does not necessarily imply that biochar active sites are less reactive than those in carbon fibers. In fact, more ordered and pure materials often have a lower active surface area, and thus lower active site density and reactivity, than materials with lower crystallinity (*e.g.*, obtained through pyrolysis at low temperature) [91,92]. Thus, linking reactivity directly to active site density is complex and extends beyond the scope of this study.

Figure 4 shows that CO desorption from thermal oxidation is underestimated by the model, although the experimental trends are still reasonably captured. At least two potential reasons can be hypothesized for the discrepancy in absolute values. First, the model currently assumes only one type of active site, corresponding to a single C-O bond strength, but surface sites are likely to be more heterogeneous, with at least two distinct types of sites identified [93,94]. In fact, Girard-Sahun *et al*. [41] included a second type of active site corresponding to a double C=O bond, which involved different desorption energies and reaction pathways. However, their kinetic scheme underestimates CO_2 desorption and overestimates CO desorption for this particular study, because a pathway to form CO_2 from C=O active sites was not included. This led us to exclude this type of active site from the kinetic scheme. Nevertheless, between 700 and 900 K, multiple CO desorption peaks observed in the experiments (see Figure 4) likely correspond to different active sites not currently included in the model. Unfortunately, it is not feasible to incorporate this inhomogeneity at this stage: even with surface characterization techniques [95], the detailed kinetics of individual active sites are largely unknown, making it difficult to quantify the influence of specific functional groups on the gasification process.

Second, our gas composition measurements reveal that H_2 and CH_4 are also desorbed from the carbon surface during the thermal oxidation experiments, as depicted in Figures 5 and 6. This can be attributed to H-containing surface groups or the presence of adsorbed H_2O. Similar H_2 desorption was found by [41] during thermogravimetric analysis of charcoal, ascribed to unavoidable H_2O adsorption on the surface after exposure to ambient air, even following drying treatment. Whether H_2 and CH_4 desorption originates from H-containing surface groups or moisture, their presence may affect surface reactivity during the thermal experiments, promoting CO desorption over CO_2. Our model cannot yet capture this

effect, as it requires knowledge of the chemistry of H-containing surface groups and/or the H_2O gasification kinetics, which are not well-characterized in the literature.

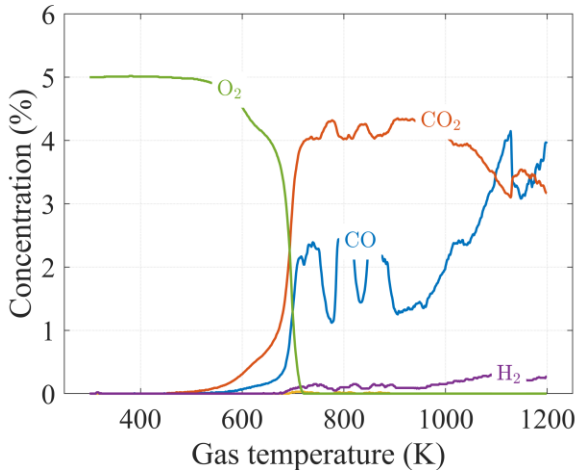

Figure 5. Species concentration as a function of gas temperature for the thermal oxidation experiment.

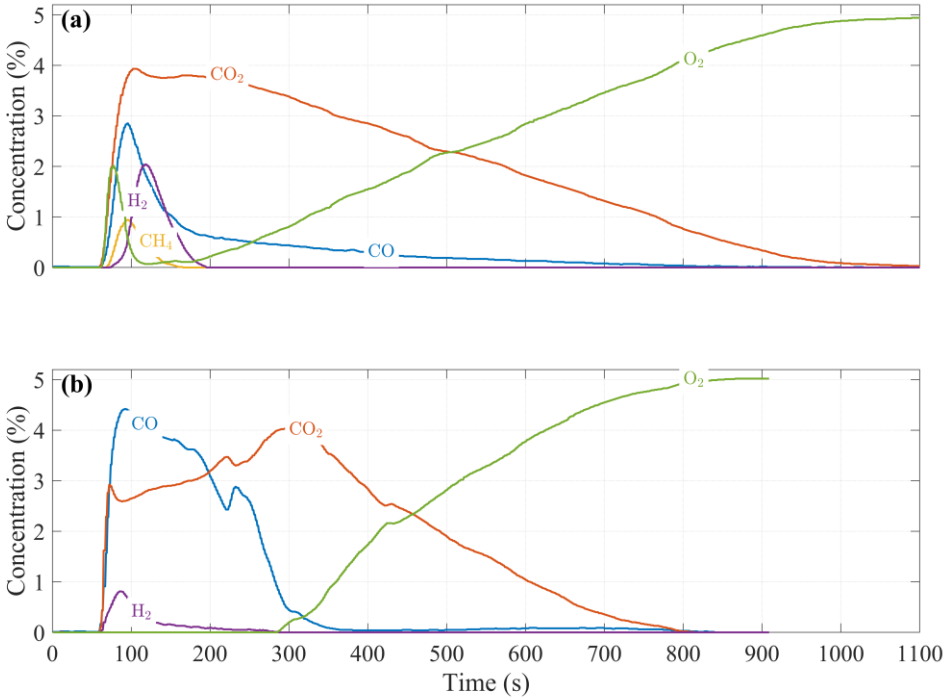

Figure 6. Species concentration as a function of time for the thermal oxidation experiments at a fixed temperature of (a) 800 and (b) 1200 K.

Notwithstanding these limitations, the model successfully captures the trends observed in the thermal experiments and can be considered calibrated with sufficient agreement. Therefore, we can now apply the model to the conditions of the main experiments in this work, specifically those combining plasma and carbon bed. The model outcome will provide valuable insights into the mechanisms underlying the performance of different configurations, helping us to better understand how reactor design influences the CO_2 conversion process.

4. Results & Discussion

4.1. Performance: Comparison between different reactors

Figure 7 presents a comparison of CO_2 conversion and EC between the three different reactors with the addition of biochar, at a flow rate of 5 L/min. Data for Reactor A in this paper were sourced from our previous work [40]. By shortening the plasma-carbon bed distance in Reactors B and C, CO_2 conversion is significantly enhanced in comparison to Reactor A. Specifically, CO_2 conversion in Reactors B and C increases by 25.4% and 52.6%, respectively, while EC reduces by 27.9% and 42.7%. Remarkably, Reactor C achieves simultaneously high CO_2 conversion (41.5%) and exceptionally low EC (2.8 eV/molecule or 278 kJ/mol, corresponding to ca. 5 GJ per tonne CO or 1.4 kWh per kilogramme CO). These values are significantly lower than those of both state-of-the-art plasma-based and conventional CO_2 splitting methods, which require about 19.5 and 34 GJ per tonne CO, respectively [69].

The improvement of reactor C, compared to reactor A and B, is likely due to the removal of the mesh that obstructs the plasma from directly contacting the biochar, allowing for more effective interactions (see the inset in Fig. 2). As a result, we achieve an EC clearly below the target necessary for plasma-based CO_2 conversion to be competitive with other technologies [3]. We would like to note that the error bars for Reactor C in Figure 7 are relatively large as a result of the direct contact between the plasma and biochar, affecting the stability of the discharge.

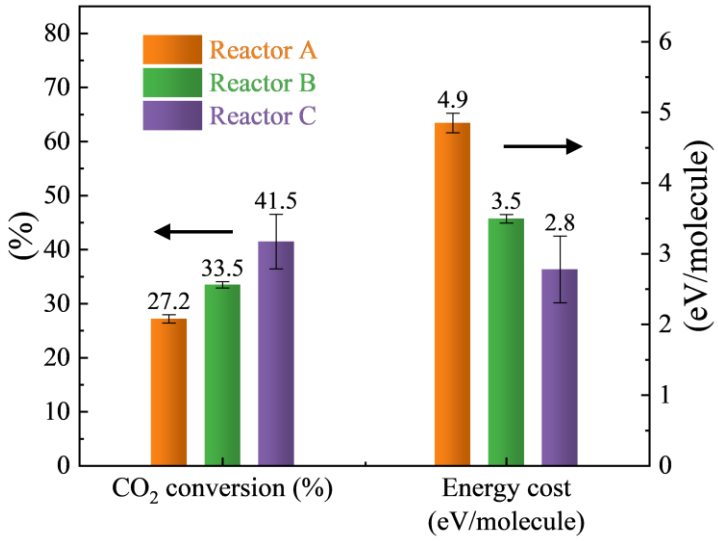

Figure 7. Comparison of CO_2 conversion, and energy cost among different reactors (CO_2 flow rate = 5 L/min). The error bars represent the standard deviation of three repeats conducted for each experimental condition.

Table 1 compares the results of our study (GAP) with other plasma setups, such as another GAP design, and also GA, MW, and DBD, without carbon bed, covering CO_2 conversion, EC, processing capacity (CO_2 inlet flow rate), and discharge power. While DBD systems can achieve a CO_2 conversion of over 40%, their processing capacity is very limited (50 mL/min), and their EC is very high (~ 80 eV/molecule) [9,10]. GA plasma offers relatively low EC (~10 eV/molecule) and higher processing capacity (3-10 L/min), but the conversion remains relatively low (about 10%) [14,15,67,68]. For MW plasma, achieving both high conversion and low EC simultaneously is also challenging [16,18,19]. In contrast, the introduction of a carbon bed after our GAP reactor (especially Reactor C) offers an optimal balance, with one of the highest CO_2 conversions (41.5%) and the lowest EC (2.8 eV/molecule), and a substantial processing capacity (5 L/min). Notably, the optimization of the plasma-carbon bed configuration in this work has significantly improved both CO_2 conversion and EC compared to previous studies of the GAP without carbon bed. Indeed, in our earlier work, the GAP alone achieved a CO_2 conversion and EC of 10.0% and 10.3 eV/molecule, respectively [40], so we see an enhanced CO_2 conversion by more than a factor four, with a simultaneous reduction in EC by a factor four.

Despite the outstanding performance of Reactor C, this configuration also exhibits limitations. One issue we encountered is that refilling the carbon bed in Reactor C is particularly challenging because the bed is almost entirely enclosed within the reactor flange, leaving very limited space to install an inlet for replenishment without fully disassembling the reactor. For larger-scale applications, we anticipate that the carbon bed design will need to be adapted to facilitate more efficient

replenishment. This could be achieved through the implementation of a silo system, as demonstrated by Girard-Sahun *et al.* [41]. In effect, a follow-up study conducted on the same reactor showed that increasing the power supplied to the system, and consequently enhancing the heat flux to the carbon bed, allows the silo system to function effectively [64]. Therefore, the improved interaction between the plasma and the carbon bed in Reactor C, providing higher temperatures, is expected to address the limited stability and long-term performance enhancement previously encountered.

4.2. Performance: Effect of the flow rate

The performance of Reactor C is further evaluated under different CO_2 flow rates, ranging from 2 to 8 L/min, and compared with Reactor A, as illustrated in Fig. 8. Both reactors exhibit a similar trend, with CO_2 conversion initially increasing and then decreasing as a function of flow rate, while EC shows the opposite trend. Specifically, the CO_2 conversion in Reactor C peaks at 44.3% at a flow rate of 3 L/min, while EC reaches a minimum of 2.6 eV/molecule at 6 L/min. Reactor C consistently outperforms Reactor A across all flow rates studied, while remaining at nearly the same SEI (cf. Fig. 8(c)). Notably, at a flow rate of 4 L/min, Reactor C exhibits an 81% improvement in CO_2 conversion (from 24.5% to 44.3%) and a 42% decrease in EC (from 5.8 eV/molecule to 3.4 eV/molecule). As biochar in the carbon bed is continuously consumed, the product composition varies with time (see Figure 8(d) below). Therefore, the conversion and EC presented in this paper represent the maximum and minimum values, respectively, as mentioned in Section 2.1. The overall variability is within ±20%, with Reactor C showing a larger variability that can be attributed to the instability of the discharge caused by the close contact between the biochar and the plasma, as mentioned in Section 4.1.

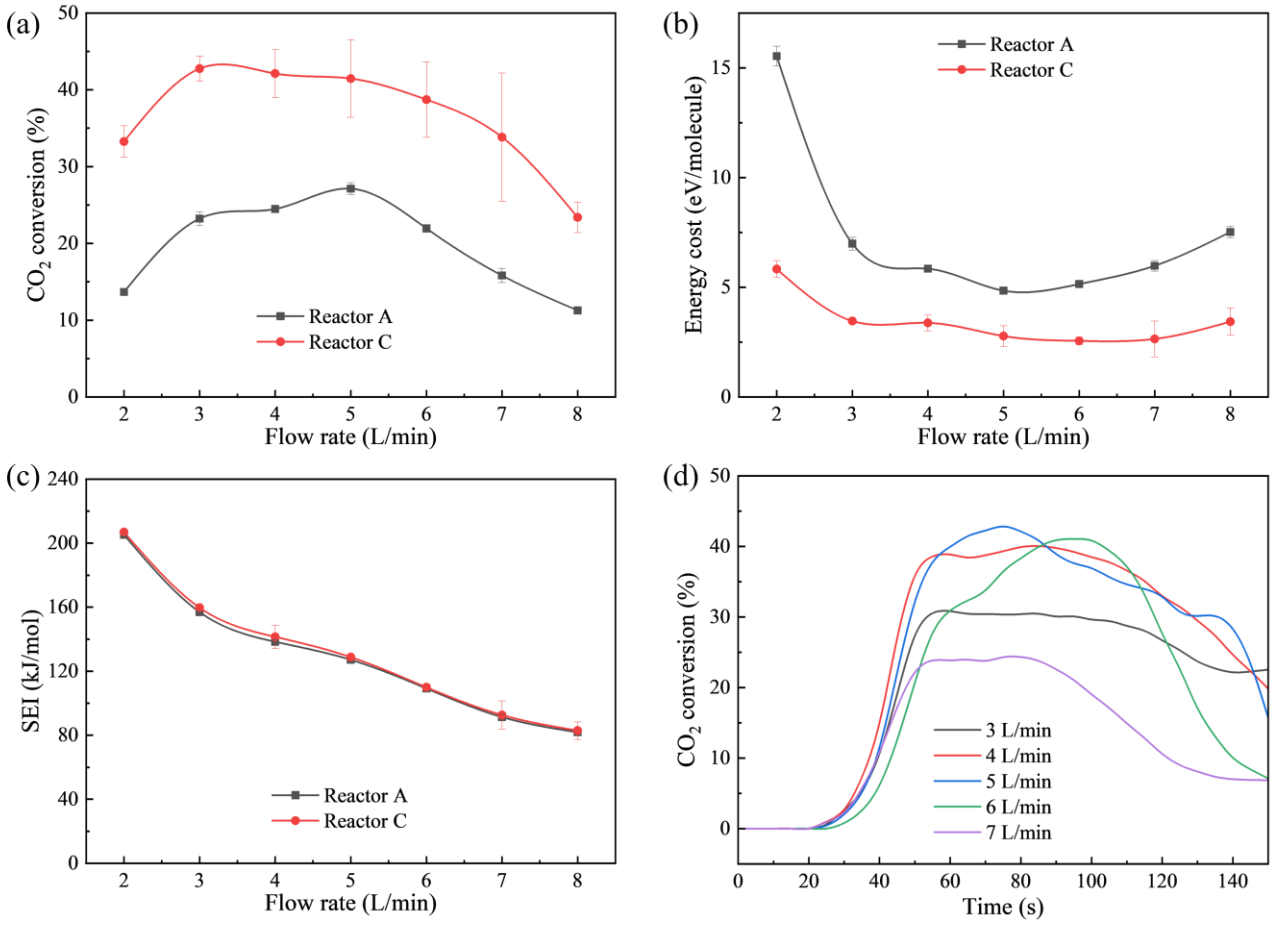

Figure 8. CO_2 conversion (a), energy cost (b) and SEI (c) as a function of CO_2 flow rate in Reactor A and C, and CO_2 conversion as a function of time in Reactor C under different flow rates (d). The error bars represent the standard deviation of three repeats conducted for each experimental condition.

4.3. Modelling: parametric sweep

Given our promising results, especially in Reactor C, we now try to understand the reasons behind the improved performance. The experiments suggest that a closer distance between the plasma and the carbon bed is beneficial, but they do not explain why, which is necessary to understand if we want to transfer our findings to other reactor setups, with the potential for upscaling. Our computational study can extract as much information as possible from the observed experimental trends. In Section 3.2, we demonstrated how the kinetic model by Girard-Sahun *et al*. [41] was adapted and calibrated for the present, new experimental conditions, and we also highlighted both its potential and the remaining limitations.

(a) Gas temperature in plasma and carbon bed

We begin the modeling study with a parametric sweep, combining different temperatures (in both the plasma and the carbon bed) and initial flow rates, to evaluate how the performance changes. Reactors A, B and C are thus approximated in the model as shown in Figure 9.

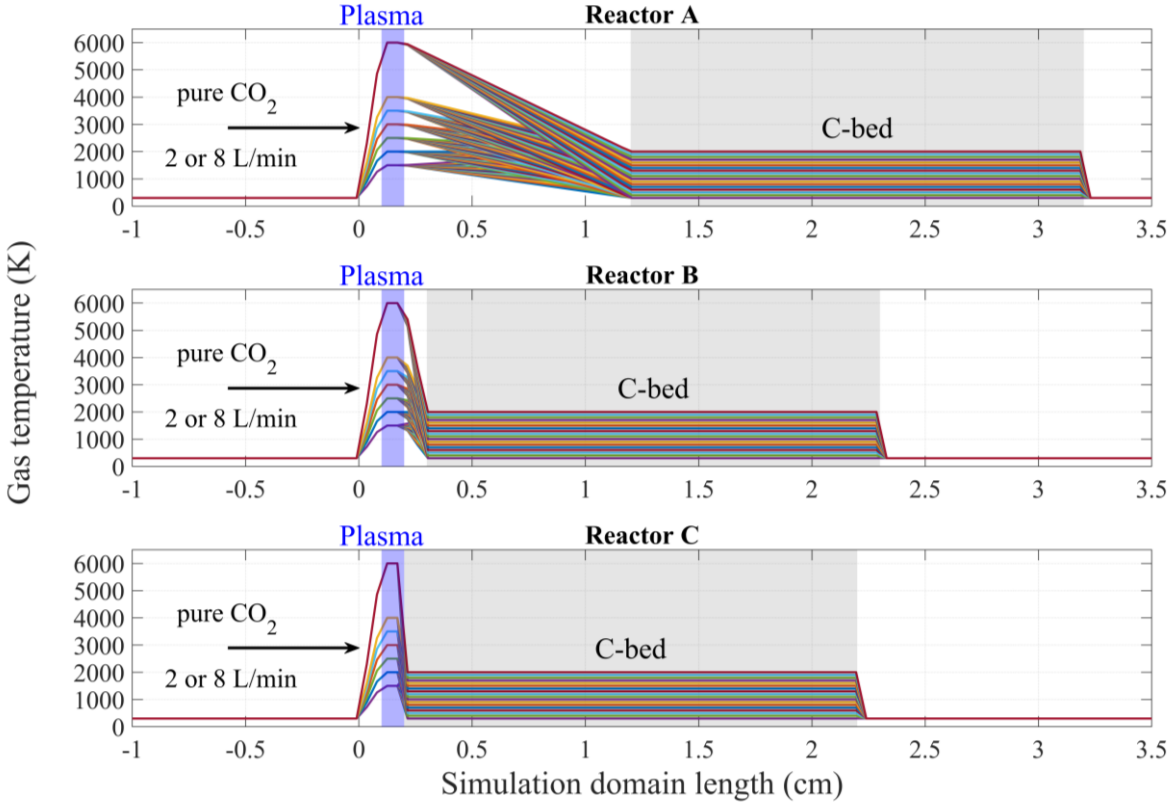

Figure 9. Schematic representation showing how reactors A, B, and C are approximated in the model, in terms of gas temperature as a function of position after the plasma. Each line corresponds to a simulation assuming a different temperature in both plasma and carbon bed. The feed gas is pure CO_2 and the initial flow rate is either 2 or 8 L/min.

In these simulations, the plasma is assumed to act as a heat source, with thermal chemistry dominating over plasma chemistry (i.e., kinetics driven by electron-impact collisions). A recent modelling investigation of the role of plasma kinetics over thermal kinetics in CO_2/CH_4 discharges by Slaets *et al*. [96] demonstrated that below 2000 K, electrons can accelerate thermal kinetics without altering the main chemical mechanisms. For temperatures above 2000 K, the effects of electrons become negligible and the kinetic scheme can be reduced to pure thermal chemistry without loss of accuracy. Therefore, the gas composition, formed in the plasma and entering the carbon bed, is determined by this thermal chemistry, based

on the gas temperature inside the plasma. The temperature inside the plasma is not known from our experiments. Measurements were attempted through optical emission spectroscopy by Zhang *et al*. [40] for reactor A, finding gas temperatures in the range of 2100−2400 K without the carbon bed. However, the measured gas temperatures are averaged along the line of sight, meaning they are not representative of the arc core and are likely significantly underestimated [97,98]. Moreover, the arc only covers a portion of the reactor's cross section, leading to substantial temperature gradients along the radial direction, from over 3000 K in the core to nearly room temperature in the surrounding swirling flow [97,98]. These gradients cannot be captured by our 0D model. For similar reasons, the temperature decay after the plasma and the temperature profile within the carbon bed are unknown and are therefore assumed to be linear and flat, respectively. Flat temperature profiles at steady state within the carbon bed were demonstrated by Girard-Sahun *et al*. [41], who measured gas temperature with thermocouples placed at different locations inside the carbon bed, finding the same values after a few minutes of operation. While these are clear approximations, particularly the discharge zone temperature, they are good enough for the purpose of our study, i.e., to obtain better insights in the effects of the carbon bed on the CO_2 conversion performance.

Given these uncertainties, we test our model using various fixed temperatures for both the arc plasma and the carbon bed, resulting in weak and strong axial temperature gradients depending on their combination (cf. the various lines in Figure 9; for reactor C, the gradient lines are not visible because we assume instant temperature decay after the plasma). The wide plasma temperature, ranging from 300 to 6000 K, is not representative for only the GAP reactor under study here, but covers most plasma sources used for CO_2 splitting operating at non-thermal and thermal regimes [3]. Thus, the insights gathered from this modelling investigation can be expanded to other plasma reactors with similar configurations. These tests also lead to different reactive mixtures entering the carbon bed: the feed gas entering the plasma is always pure CO_2, which then decomposes in the arc plasma based on the arc temperature, as explained above. The dissociation products either recombine to form again CO_2 or undergo further reactions in the afterglow, depending on the cooling rate and the length of this stage (i.e., distance between plasma and carbon bed). As we cannot simulate the mesh that separates the plasma from the carbon bed in reactor B, we assume an arbitrary distance of 1 mm. Additionally, we test an arc temperature of 1500 K, which leads to no CO_2 conversion before entering the carbon bed, as a benchmark representing pure thermal gasification (without plasma) to complete the parametric study.

The results of our parametric study for each reactor configuration are presented in the following two sections. In particular, we use the conversion improvement and O_2 removal efficiency as performance metrics.

(b) Conversion improvement as a function of CO_2 conversion before the carbon bed and carbon bed temperature

The conversion improvement is calculated by subtracting the final conversion of the simulation with an empty carbon bed from the final conversion of the simulation with carbon bed filled with fresh carbon, and it is plotted in Figure 10, as a function of both the CO_2 conversion before the carbon bed and the temperature at the carbon bed. Note that our simulations not always predict improvement in conversion due to the carbon bed; sometimes the conversion is lower with filled carbon bed (as explained below), so we plot the difference in conversion, with red and blue values indicating that the conversion is better or worse than for an empty carbon bed, respectively, and the dashed line separates both regions.

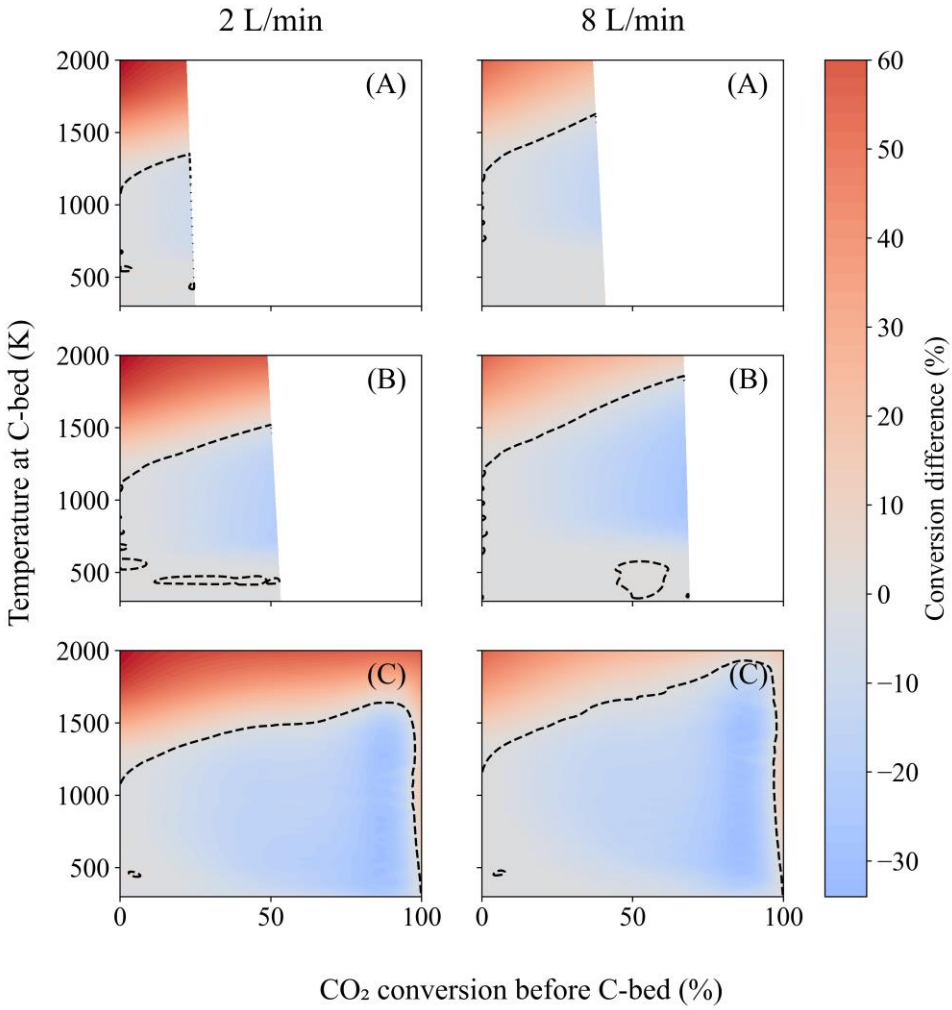

Figure 10. Conversion difference between simulations with filled carbon bed and with empty carbon bed, as a function of both CO_2 conversion before the carbon bed and temperature at the carbon bed, for Reactors A, B and C (as indicated by the annotations inside the subplots) and initial flow rate of 2 and 8 L/min. The dashed contour line divides between positive (red) and negative (blue) values.

By comparing the various plots in Figure 10, we observe that the closer the plasma is to the carbon bed, the wider is the range of CO_2 conversion in the mixture entering the carbon bed (cf. reactor C vs reactor B and A). Indeed, in reactor A, with a 10 mm gap between plasma and carbon bed, most of the CO_2 dissociation achieved in the plasma zone is lost already when entering the carbon bed, resulting in a maximum CO_2 conversion of approximately 25% at 2 L/min and around 40% at 8 L/min. Reducing the distance to 1 mm (reactor B) increases this maximum conversion to around 55% and 70%, respectively, while direct contact in reactor C allows for a fully dissociated mixture entering the carbon bed at both initial flow rates. This difference between the three configurations arises from the length of the afterglow: the longer the afterglow, the more time the dissociation products have to recombine and form again CO_2.

Furthermore, we observe that the maximum CO_2 conversion (or dissociation degree) of the mixture entering the carbon bed tends to slightly decrease with increasing temperature at the carbon bed for the same reactor and flow rate. This happens because a higher carbon bed temperature slows down the temperature decay in the afterglow, promoting recombination reactions. This issue is mitigated when the hot plasma zone is in direct contact with the carbon bed in reactor C.

Additionally, when comparing the flow rates of 2 and 8 L/min for the same reactor, we see that the maximum dissociation degree of the mixtures entering the carbon bed increases with flow rate, as also mentioned above. This is due to the shorter residence time in the afterglow, which reduces the impact of recombination reactions.

The maximum CO_2 conversion obtained in the simulations is highly dependent on the temperatures set in the plasma and carbon bed zones, as well as the spatial separation between them. The simulations predict a maximum conversion of nearly 100% in Reactor C when a plasma temperature of 6000 K and a carbon bed temperature of 300 K are used. However, these values represent extreme conditions that are practically unattainable, as they assume direct contact between the hot plasma and a room-temperature carbon bed. Under more realistic conditions, resembling those of our experiments, such as an arc temperature of 3000 K and a carbon bed temperature of 1500 K, the simulations predict a maximum conversion of approximately 45% at a flow rate of 2 L/min in Reactor C. This result aligns well with our experimental maximum of 41.5% for a flow rate of 5 L/min.

In effect, the color patterns in Figure 10 indicate that high conversion before the carbon bed is only beneficial if a very high temperature (>1600 K) can be maintained; otherwise, the oxidation of oxygen complexes to CO_2 dominates (O + C(O)s → CO_2 and O_2 + C(O)s → CO_2 + O, with C(O)s being an oxygen complex at the surface [41]), leading to a drop in conversion compared to empty carbon bed (cf. blue region). Thus, the higher the dissociation degree before the carbon bed, the higher must be the temperature in the carbon bed to observe a beneficial effect. Overall, it is clear that an improvement in CO_2 conversion due to the carbon bed is only obtained at carbon bed temperatures above ca. 1400-1600 K.

(c) O_2 removal as a function of CO_2 conversion before the carbon bed and carbon bed temperature

The explanation for the drop in CO_2 conversion due to oxidation of oxygen complexes to CO_2 at the carbon bed is even more evident when looking at the O_2 percentage left in the product stream after the carbon bed (inversely proportional to the O_2 removal efficiency) as a function of both the CO_2 conversion before the carbon bed and the temperature at the carbon bed, in Figure 11.

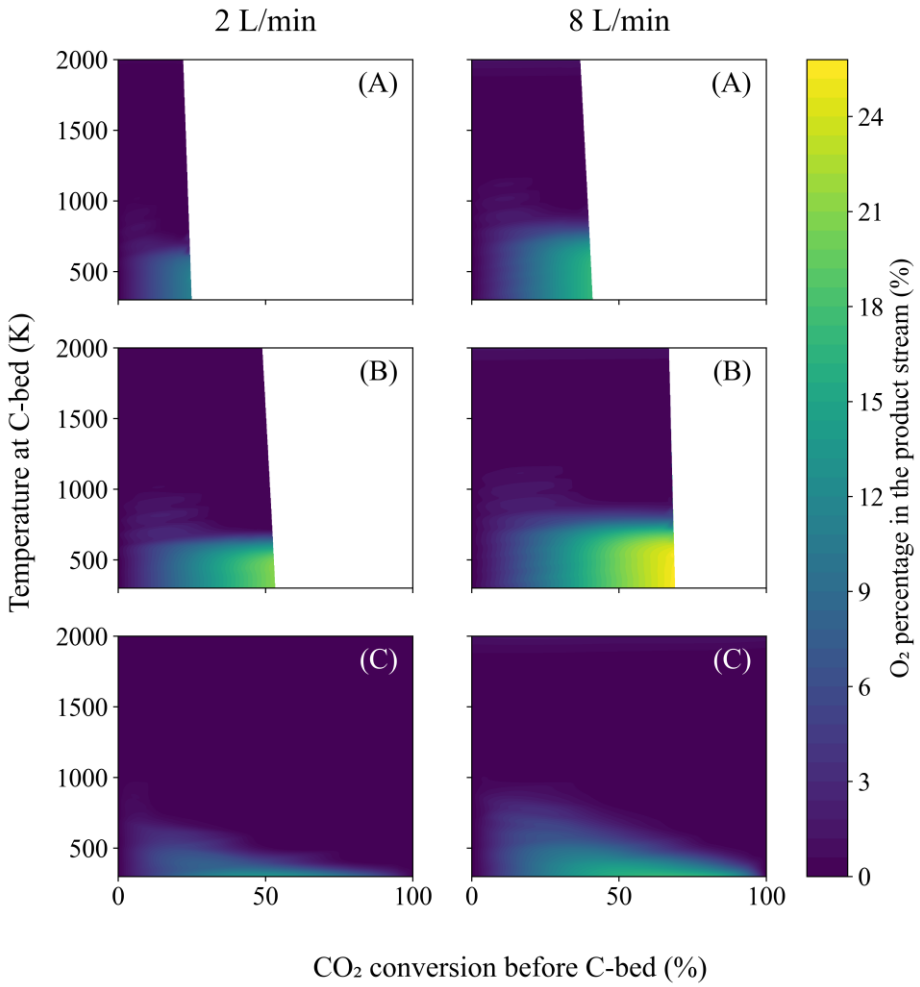

Figure 11. O_2 percentage left in the product stream after the carbon bed as a function of both CO_2 conversion before the carbon bed and temperature at the carbon bed, for reactors A, B and C (as indicated by the annotations inside the subplots) and initial flow rate of 2 and 8 L/min.

If we compare Figure 10 with Figure 11, we observe that despite the detrimental effect on CO_2 conversion for carbon bed temperatures below 1400-1600 K, O_2 is fully removed from the product mixture at temperatures above 600 K. This indicates that the detrimental effect on conversion cannot be explained by the complete consumption or deactivation of the carbon bed. As noted by Girard-Sahun *et al*. [41], the detrimental effect should be attributed to the efficient conversion of O_2 into CO_2, promoting the full oxidation of carbon. The reasons for this will be explored in more detail in the next section, where we will conduct a deeper analysis of the reactions under specific conditions of interest.

Before moving to the next section, we can observe that the temperature required to remove all O_2 from the mixture is significantly lower in reactor C (i.e., around 400 K, while it is ca. 600 K for reactors A and B). This occurs because in reactors A and B, the afterglow is long enough for almost complete recombination of O atoms into O_2 and CO_2 before reaching the carbon bed. However, in Reactor C, the direct contact with the plasma allows O atoms to attack the carbon surface directly, with virtually barrierless adsorption, whereas O_2 faces an activation barrier (~0.7 eV) due to the cleavage of the double bond. This mechanism will also be clarified in the next section.

4.4. Modelling: Reaction analysis

(a) Importance of reverse Boudouard reaction vs full oxidation of carbon into CO_2: Different behavior at high vs low carbon bed temperature

In this section, we delve deeper into the mechanisms highlighted in the previous section through reaction analysis. The first mechanism we will examine is the full oxidation of carbon into CO_2 due to an excess of O_2, which occurs when the temperature in the carbon bed is too low (i.e., below ca. 1500 K for reactors A, B and C, as indicated by the dashed lines in Fig. 10). To explore this, we compare two different conditions in Reactor B: a bed temperature of 1000 K and 1800 K. These temperatures are selected due to their distinctly different impacts on reaction pathways. At 1000 K, the temperature promotes carbon oxidation but is insufficient to drive RBR. In contrast, at 1800 K, the temperature is high enough to enhance the beneficial effects of the carbon bed on CO_2 conversion performance across most experimental conditions, as illustrated in Figure 10. The main net reaction rates for these two conditions are plotted as a function of position in both plasma and carbon bed, in Figure 12 (a,b).

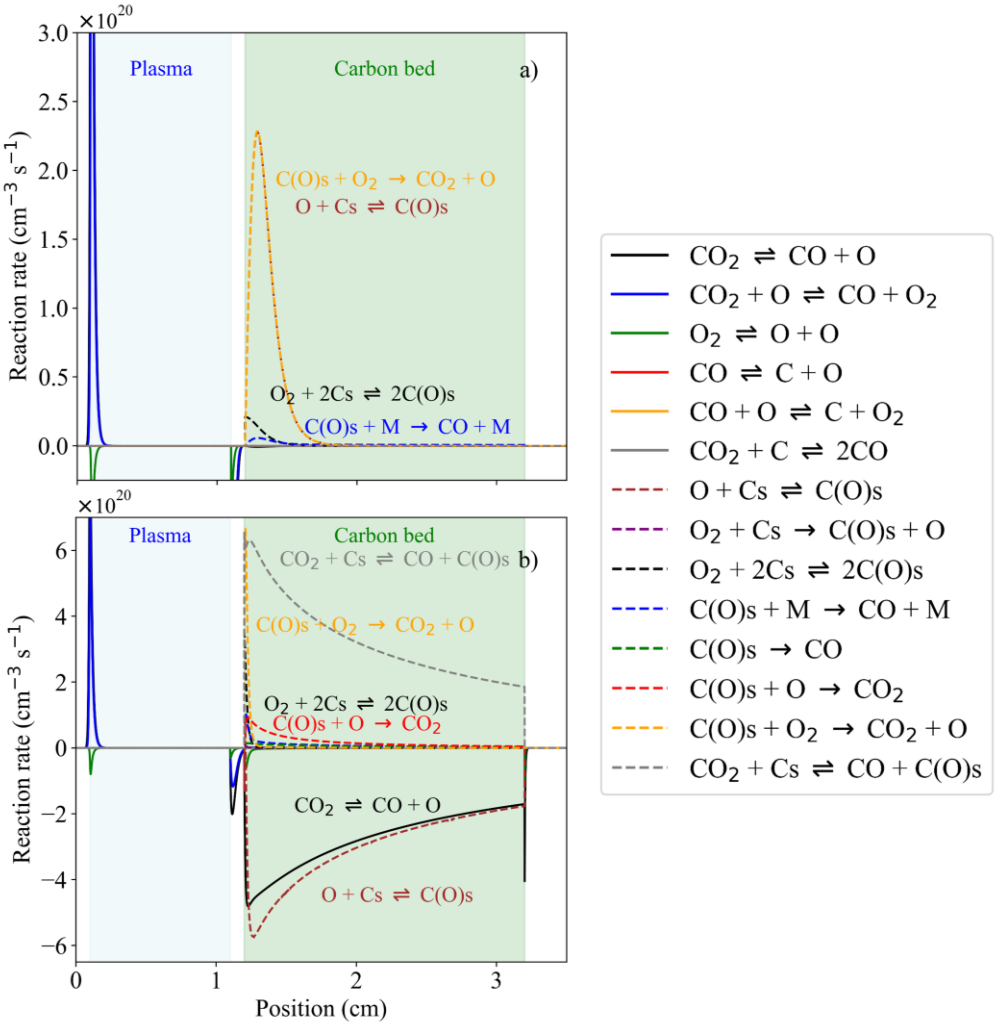

Figure 12. Net rates of the main gas-phase (solid lines) and surface (dashed lines) reactions as a function of position in plasma and carbon bed, for reactor B, at a plasma temperature of 3000 K and a carbon bed temperature of 1000 K (a) and 1800 K (b). The reactions with negative reaction rates proceed to the left.

If we compare panel (a) and (b), we observe that the scale of the reaction rates significantly increases when moving from a carbon bed temperature of 1000 K to 1800 K. This occurs because, at higher temperatures, the carbon bed becomes more reactive, and additional reaction pathways are activated. At 1800 K, the reverse Boudouard reaction (RBR: CO_2 + Cs ⇌ CO + C(O)s) plays a dominant role in the kinetics (grey dashed line in (b)), whereas it is completely absent at 1000 K. The RBR should then be accompanied by spontaneous (C(O)s → CO) or collision-induced (C(O)s + M → CO + M) CO desorption, to obtain two CO molecules from a CO_2 molecule. However, Figure 12 indicates that their rates are small compared to reactions involving O_2. In effect, at temperatures well above 600 K, O_2 is rapidly removed from the gas phase as soon as it contacts the carbon bed, generating a large number of surface oxygen complexes, i.e., C(O)s. At 1800 K, these complexes are unstable and release O atoms back into the gas phase (yellow dashed line, which peaks in the beginning of the carbon bed, as well as brown dashed line, with negative values in (b), indicating that it proceeds to the left, hence also producing O atoms). These O atoms then efficiently oxidize the surface complexes, forming again CO_2 (red dashed line in (b)). Simultaneously, CO is reoxidized by O atoms, cf. black solid line in (b), proceeding in the reverse direction, hence further producing CO_2.

However, the rate of the RBR exceeds the oxidation rates as soon as O_2 is fully consumed within ca. 0.2 cm in the carbon bed (cf. grey dashed line vs red dashed line and black solid line in (b)), leading to a net CO_2 conversion rate at the carbon bed and explaining the beneficial effect of the carbon bed at 1800 K. This is well visible in Figure 13 in which only the reactions directly involving CO_2 are plotted as a function of position for reactor B, with a net CO_2 conversion inside the plasma, net recombination in the afterglow and in the first 0.5 mm of the carbon bed, but further net CO_2 conversion in

the carbon bed. Immediately downstream of the carbon bed, another pronounced peak in net CO_2 formation is observed. This is attributed to the recombination of unreacted O atoms with CO, forming again CO_2. The presence of these unreacted O atoms stems from the high instability of oxygen complexes at 1800 K, a temperature at which O atoms undergo continuous adsorption and desorption cycles.

In contrast, at 1000 K, the RBR is not activated, so the oxygen complexes formed upon O_2 adsorption are only oxidized to CO_2 (yellow dashed line in (a), which occurs after the formation of C(O)s, i.e., brown dashed line in (a)), and this reduces the performance to levels even below the benchmark case (i.e., with empty carbon bed).

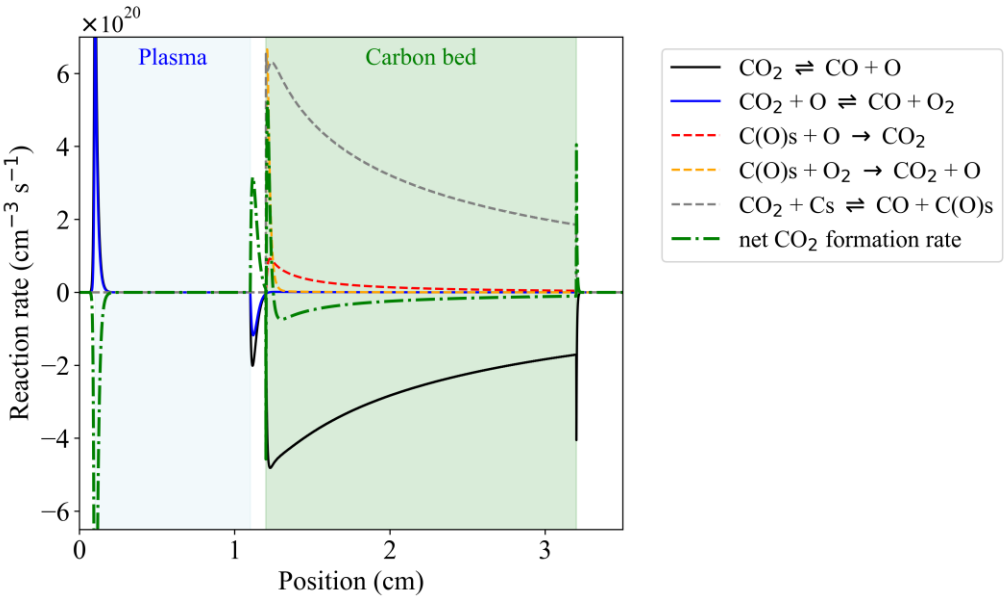

Figure 13. Net rates of the main gas-phase (solid lines) and surface (dashed lines) reactions producing or consuming CO_2 as a function of position in plasma and carbon bed, for reactor B, at a plasma temperature of 3000 K and a carbon bed temperature of 1800 K. The net CO_2 formation/dissociation rate is also plotted, with negative values denoting net CO_2 dissociation and positive values net CO_2 production, for clarity in the figure.

Another insight we gain from Figure 12 is that the kinetics quickly equilibrate within the plasma, with all net reaction rates approaching zero after the initial peaks of the blue and green solid lines. However, as soon as the gas enters the afterglow, the net rates turn negative due to recombination reactions, i.e., blue and black solid line (recombination of CO with O or O_2 into CO_2) and green solid line (recombination of two O atoms into O_2).

(b) O atoms can activate carbon bed at lower temperatures

Figure 14 shows the net reaction rates as a function of position in plasma and carbon bed for reactor C, where the plasma temperature is 6000 K and the carbon bed temperature is 400 K. The higher plasma temperature compared to Figure 12 is selected to maximize the fraction of O atoms entering the carbon bed, while the 400 K carbon bed temperature is chosen to emphasize that O atom adsorption can occur near room temperature. While having a very hot plasma in direct contact with a cold carbon bed is unlikely in an experimental setup (since the carbon bed would inevitably be heated by the plasma) this extreme scenario provides valuable insights into the effects of combining mixtures with un-recombined O atoms and a cold carbon bed.

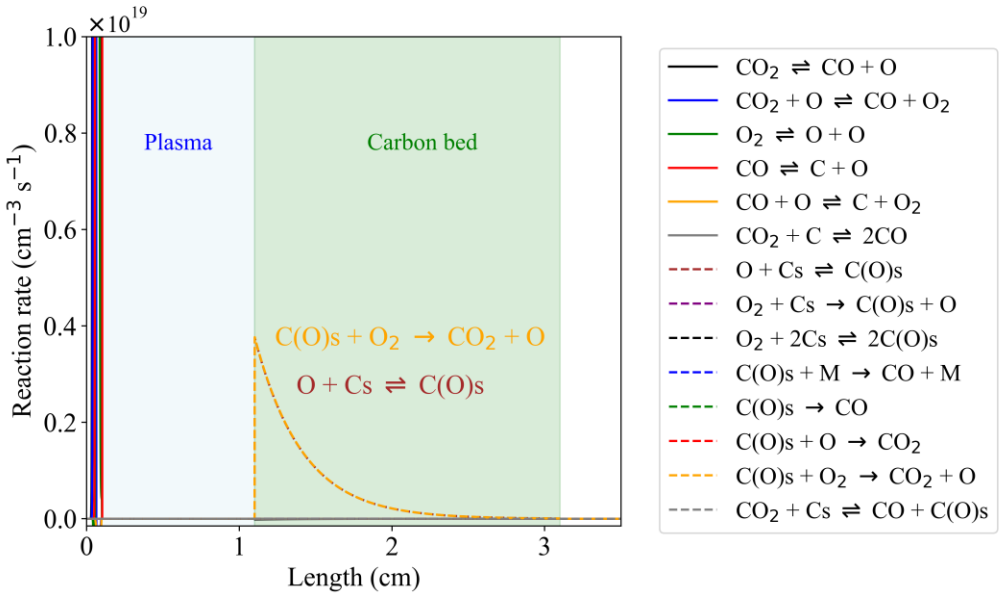

Figure 14. Net rates of the main gas-phase (solid lines) and surface (dashed lines) reactions as a function of position in the plasma and carbon bed, for Reactor C, at a plasma temperature of 6000 K and a carbon bed temperature of 400 K.

First of all, we do not observe negative rates in Figure 14, due to recombination in the afterglow. This can be explained by the close contact between the plasma and the carbon bed, so that the afterglow occurs within the carbon bed itself. As a result, O atoms, which are the primary drivers of recombination reactions, are rapidly adsorbed by the carbon surface with virtually no barrier for adsorption (brown dashed line). These atoms are then sequestered by the surface due to the lower temperatures in the carbon bed. At much higher temperatures, however, the oxygen complexes formed on the surface would become weaker, allowing some O atoms to be released back into the gas phase, as shown in Figure 12(b).

The formation of these surface oxygen complexes, C(O)s, triggers the consumption of O_2 (yellow dashed line), which must overcome an activation barrier due to the breaking of the O=O double bond. Because of the presence of these oxygen complexes, O_2 can be consumed at lower temperatures than would be possible with fresh carbon surfaces, such as those in Reactors A and B. In these reactors, the afterglow before the carbon bed leads to recombination reactions that consume nearly all O atoms, so only O_2 reaches the carbon surface, increasing the temperature needed to observe the removal of O/O_2 from the product mixture. This suggests that if one aims to fully remove O_2 from the exhaust, but the waste heat from the plasma cannot sufficiently heat the carbon bed, using a partially oxidized carbon material could overcome the issue of O_2 separation, albeit without necessarily improving the conversion performance.

5. Conclusions

Warm plasmas, such as GA and MW discharges, provide promising solutions for electrification of the chemical industry. However, their implementation still faces EC challenges, which are not yet aligned with industrial standards. Specifically for CO_2 conversion into CO, a key area for improvement is the management of recombination reactions that form again CO_2 after the plasma. Even if nearly complete dissociation is achieved in the hot plasma zone, downstream dissociation is limited to, or below the thermodynamic limit, unless specific modifications are adopted to suppress recombination reactions, such as the addition of quenching nozzles.

An alternative approach that has shown promise in recent years is the addition of a carbon bed downstream of the hot plasma zone. This setup helps convert O/O_2 (competing products) into additional CO (the desired product), thus shifting the equilibrium towards more favorable products. This coupling not only improves conversion and reduces EC of the process, but also serves as a model for plasma-assisted gasification of carbon-rich waste materials.

In this study, we advance plasma-based CO_2 conversion by exploring different configurations for coupling plasma with a carbon bed. The original configuration, which serves as a benchmark, was developed and studied by Zhang *et al*. [40]. Here, we reduce the distance between the plasma and carbon bed and also reverse the setup to remove the mesh holding the carbon pellets in place, allowing direct contact between the plasma and the solid carbon. These two new configurations lead to drastic improvements, with the latter achieving CO_2 conversion exceeding 40% and an EC below 2.8 eV/molecule (or 278 kJ/mol, corresponding to ca. 5 GJ per tonne CO or 1.4 kWh per kilogramme CO). This represents over a fourfold increase in conversion and almost a fourfold reduction in EC compared to the benchmark experiment, i.e., plasma without carbon bed. These results are particularly impressive when compared to the state of the art for plasma-based CO_2 splitting [3,99], where achieving conversion higher than 40% typically requires an order of magnitude more energy per molecule. Furthermore, our best results make it even more evident that plasma-driven RBR can surpass the performance of conventional and competing technologies for CO_2 conversion, such as CO_2 electrolysis, particularly in terms of reducing the EC for CO production.

We explain this remarkable performance through detailed kinetic modeling, which shows that closer contact with the hot plasma zone enables higher temperatures that favor the reverse Boudouard reaction. Our model also reveals that the carbon bed is not effective at quenching recombination reactions into CO_2, as O/O_2 is primarily converted into CO_2. However, for carbon bed temperatures higher than 1500 K, the reverse Boudouard reaction significantly enhances CO_2 conversion, compensating for the detrimental effects of recombination reactions. Additionally, O atoms can drive efficient O_2 removal even at lower carbon bed temperatures, but without sustaining high temperatures, oxidation dominates, counteracting the positive effects of the carbon bed. These findings suggest that the use of a carbon bed is particularly beneficial for setups with moderate performance and significant heat losses to reactor walls. However, for reactors that already achieve high conversion, maintaining high temperatures at the carbon bed is crucial; otherwise, oxidation is promoted, and the beneficial effects of the carbon bed are lost.

To conclude, we emphasize the importance of conducting detailed techno-economic and lifecycle assessments to evaluate the feasibility and scalability of plasma-driven RBR reactors. While both a techno-economic analysis [69] and sustainability assessment [70] have previously been performed for a similar (GAP) reactor with post-plasma carbon bed, no comprehensive analysis has yet been carried out for the specific system studied here. In general terms, plasma-driven RBR offers several advantages over alternative technologies. It operates independently of fossil fuels and does not require water consumption, unlike electrolysis-based systems, nor does it rely on costly reactants or materials for reactor construction. The technology is compatible with renewable energy sources, further enhancing its environmental sustainability. Notably, the inherent recycling loop for unreacted CO_2 promotes a circular material flow, contrasting with the linear, non-restorative process of partial fossil fuel combustion. In addition, biochar is a renewable source of carbon and promotes a closed-loop system by converting biomass waste into valuable products. These characteristics position plasma-driven RBR as a promising technology for the energy transition. However, a comprehensive evaluation of the energy input required for the entire process, including plasma generation and carbon bed maintenance, is essential to validate its potential and fully substantiate these results.

CRediT authorship contribution statement

Omar Biondo: Writing – original draft, Methodology, Investigation, Conceptualization. **Kaiyi Wang**: Writing – original draft, Methodology, Investigation, Conceptualization. **Hao Zhang**: Writing – review & editing, Supervision, Funding acquisition. **Annemie Bogaerts**: Writing – review & editing, Supervision, Funding acquisition.

Acknowledgments

We gratefully acknowledge financial support by the Fund for Scientific Research (FWO; grant ID 1205424N), the European Research Council (ERC) under the European Union's Horizon 2020 research and innovation programme (grant agreement no. 810182; SCOPE ERC Synergy project), the VLAIO-Catalisti ICON project "BluePlasma" (grant ID HBC.2022.0445), and the National Natural Science Foundation of China (NSFC, grant ID 52276214).

References

[1] C. Hepburn, E. Adlen, J. Beddington, E.A. Carter, S. Fuss, N. Mac Dowell, J.C. Minx, P. Smith, C.K. Williams, The technological and economic prospects for CO2 utilization and removal, Nature 575 (2019) 87–97. https://doi.org/10.1038/s41586-019-1681-6.

[2] V. Dieterich, A. Buttler, A. Hanel, H. Spliethoff, S. Fendt, Power-to-liquid *via* synthesis of methanol, DME or Fischer–Tropsch-fuels: a review, Energy Environ. Sci. 13 (2020) 3207–3252. https://doi.org/10.1039/D0EE01187H.

[3] R. Snoeckx, A. Bogaerts, Plasma technology – a novel solution for CO_2 conversion?, Chem. Soc. Rev. 46 (2017) 5805–5863. https://doi.org/10.1039/C6CS00066E.

[4] R.R. Ratnakar, Decarbonizing hydrogen supply chain via electrifying endothermic processes, Chemical Engineering Science 299 (2024) 120439. https://doi.org/10.1016/j.ces.2024.120439.

[5] W.-C. Chung, M.-B. Chang, Review of catalysis and plasma performance on dry reforming of CH4 and possible synergistic effects, Renewable and Sustainable Energy Reviews 62 (2016) 13–31. https://doi.org/10.1016/j.rser.2016.04.007.

[6] M. Scapinello, E. Delikonstantis, G.D. Stefanidis, The panorama of plasma-assisted non-oxidative methane reforming, Chemical Engineering and Processing: Process Intensification 117 (2017) 120–140. https://doi.org/10.1016/j.cep.2017.03.024.

[7] G.J. Van Rooij, H.N. Akse, W.A. Bongers, M.C.M. Van De Sanden, Plasma for electrification of chemical industry: a case study on CO_2 reduction, Plasma Phys. Control. Fusion 60 (2018) 014019. https://doi.org/10.1088/1361-6587/aa8f7d.

[8] A. Bogaerts, E.C. Neyts, Plasma Technology: An Emerging Technology for Energy Storage, ACS Energy Lett. 3 (2018) 1013–1027. https://doi.org/10.1021/acsenergylett.8b00184.

[9] Y. Uytdenhouwen, S. Van Alphen, I. Michielsen, V. Meynen, P. Cool, A. Bogaerts, A packed-bed DBD micro plasma reactor for CO2 dissociation: Does size matter?, Chemical Engineering Journal 348 (2018) 557–568. https://doi.org/10.1016/j.cej.2018.04.210.

[10] B. Wang, X. Wang, H. Su, Influence of Electrode Interval and Barrier Thickness in the Segmented Electrode Micro-plasma DBD Reactor on CO2 Decomposition, Plasma Chem Plasma Process 40 (2020) 1189–1206. https://doi.org/10.1007/s11090-020-10091-1.

[11] M.S. Moss, K. Yanallah, R.W.K. Allen, F. Pontiga, An investigation of CO_2 splitting using nanosecond pulsed corona discharge: effect of argon addition on CO_2 conversion and energy efficiency, Plasma Sources Sci. Technol. 26 (2017) 035009. https://doi.org/10.1088/1361-6595/aa5b1d.

[12] C. Montesano, T.P.W. Salden, L.M. Martini, G. Dilecce, P. Tosi, CO_2 Reduction by Nanosecond-Plasma Discharges: Revealing the Dissociation's Time Scale and the Importance of Pulse Sequence, J. Phys. Chem. C 127 (2023) 10045–10050. https://doi.org/10.1021/acs.jpcc.3c02547.

[13] T. Yong, H. Zhong, E. Pannier, C. Laux, M.A. Cappelli, High-pressure CO_2 dissociation with nanosecond pulsed discharges, Plasma Sources Sci. Technol. 32 (2023) 115012. https://doi.org/10.1088/1361-6595/ad066e.

[14] M. Ramakers, G. Trenchev, S. Heijkers, W. Wang, A. Bogaerts, Gliding Arc Plasmatron: Providing an Alternative Method for Carbon Dioxide Conversion, ChemSusChem 10 (2017) 2642–2652. https://doi.org/10.1002/cssc.201700589.

[15] S.R. Sun, H.X. Wang, D.H. Mei, X. Tu, A. Bogaerts, CO 2 conversion in a gliding arc plasma: Performance improvement based on chemical reaction modeling, Journal of CO2 Utilization 17 (2017) 220–234. https://doi.org/10.1016/j.jcou.2016.12.009.

[16] L.F. Spencer, A.D. Gallimore, CO_2 dissociation in an atmospheric pressure plasma/catalyst system: a study of efficiency, Plasma Sources Sci. Technol. 22 (2012) 015019. https://doi.org/10.1088/0963-0252/22/1/015019.

[17] W. Bongers, H. Bouwmeester, B. Wolf, F. Peeters, S. Welzel, D. van den Bekerom, N. den Harder, A. Goede, M. Graswinckel, P.W. Groen, J. Kopecki, M. Leins, G. van Rooij, A. Schulz, M. Walker, R. van de Sanden, Plasma-driven

dissociation of CO_2 for fuel synthesis, Plasma Process Polym 14 (2017) 1600126. https://doi.org/10.1002/ppap.201600126.
[18] D. Mansfeld, S. Sintsov, N. Chekmarev, A. Vodopyanov, Conversion of carbon dioxide in microwave plasma torch sustained by gyrotron radiation at frequency of 24 GHz at atmospheric pressure, Journal of CO2 Utilization 40 (2020) 101197. https://doi.org/10.1016/j.jcou.2020.101197.
[19] Y. Qin, G. Niu, X. Wang, D. Luo, Y. Duan, Conversion of CO2 in a low-powered atmospheric microwave plasma: In-depth study on the trade-off between CO2 conversion and energy efficiency, Chemical Physics 538 (2020) 110913. https://doi.org/10.1016/j.chemphys.2020.110913.
[20] A. Hecimovic, F.A. D'Isa, E. Carbone, U. Fantz, Enhancement of CO2 conversion in microwave plasmas using a nozzle in the effluent, Journal of CO2 Utilization 57 (2022) 101870. https://doi.org/10.1016/j.jcou.2021.101870.
[21] S. Kelly, C. Verheyen, A. Cowley, A. Bogaerts, Producing oxygen and fertilizer with the Martian atmosphere by using microwave plasma, Chem 8 (2022) 2797–2816. https://doi.org/10.1016/j.chempr.2022.07.015.
[22] A. Fridman, Plasma Chemistry, Cambridge: Cambridge University Press, 2008.
[23] A. Bogaerts, T. Kozák, K. van Laer, R. Snoeckx, Plasma-based conversion of CO_2 : current status and future challenges, Faraday Discuss. 183 (2015) 217–232. https://doi.org/10.1039/C5FD00053J.
[24] O. Biondo, C. Fromentin, T. Silva, V. Guerra, G. Van Rooij, A. Bogaerts, Insights into the limitations to vibrational excitation of CO_2 : validation of a kinetic model with pulsed glow discharge experiments, Plasma Sources Sci. Technol. 31 (2022) 074003. https://doi.org/10.1088/1361-6595/ac8019.
[25] R.I. Azizov, A.K. Vakar, V.K. Zhivotov, M.F. Krotov, O.A. Zinovev, B.V. Potapkin, A.A. Rusanov, V.D. Rusanov, A.A. Fridman, Nonequilibrium plasmachemical process of CO2 decomposition in a supersonic microwave discharge, Akademiia Nauk SSSR Doklady 271 (1983) 94–98.
[26] N. den Harder, D.C.M. van den Bekerom, R.S. Al, M.F. Graswinckel, J.M. Palomares, F.J.J. Peeters, S. Ponduri, T. Minea, W.A. Bongers, M.C.M. van de Sanden, G.J. van Rooij, Homogeneous CO_2 conversion by microwave plasma: Wave propagation and diagnostics, Plasma Process Polym 14 (2017) 1600120. https://doi.org/10.1002/ppap.201600120.
[27] G. Chen, N. Britun, T. Godfroid, V. Georgieva, R. Snyders, M.-P. Delplancke-Ogletree, An overview of CO_2 conversion in a microwave discharge: the role of plasma-catalysis, J. Phys. D: Appl. Phys. 50 (2017) 084001. https://doi.org/10.1088/1361-6463/aa5616.
[28] C.M. Mitsingas, R. Rajasegar, S. Hammack, H. Do, T. Lee, High Energy Efficiency Plasma Conversion of CO_2 at Atmospheric Pressure Using a Direct-Coupled Microwave Plasma System, IEEE Trans. Plasma Sci. 44 (2016) 651–656. https://doi.org/10.1109/TPS.2016.2531641.
[29] H. Kim, S. Song, C.P. Tom, F. Xie, Carbon dioxide conversion in an atmospheric pressure microwave plasma reactor: Improving efficiencies by enhancing afterglow quenching, Journal of CO2 Utilization 37 (2020) 240–247. https://doi.org/10.1016/j.jcou.2019.12.011.
[30] A. Hecimovic, C.K. Kiefer, A. Meindl, R. Antunes, U. Fantz, Fast gas quenching of microwave plasma effluent for enhanced CO2 conversion, Journal of CO2 Utilization 71 (2023) 102473. https://doi.org/10.1016/j.jcou.2023.102473.
[31] E.R. Mercer, S. Van Alphen, C.F.A.M. Van Deursen, T.W.H. Righart, W.A. Bongers, R. Snyders, A. Bogaerts, M.C.M. Van De Sanden, F.J.J. Peeters, Post-plasma quenching to improve conversion and energy efficiency in a CO2 microwave plasma, Fuel 334 (2023) 126734. https://doi.org/10.1016/j.fuel.2022.126734.
[32] R.J. Detz, B. Van Der Zwaan, Cost projections for microwave plasma CO production using renewable energy, Journal of Energy Chemistry 71 (2022) 507–513. https://doi.org/10.1016/j.jechem.2022.04.014.
[33] C. O'Modhrain, G. Trenchev, Y. Gorbanev, A. Bogaerts, Upscaling Plasma-Based CO_2 Conversion: Case Study of a Multi-Reactor Gliding Arc Plasmatron, ACS Eng. Au 4 (2024) 333–344. https://doi.org/10.1021/acsengineeringau.3c00067.
[34] R. Vertongen, A. Bogaerts, How important is reactor design for CO2 conversion in warm plasmas?, Journal of CO2 Utilization 72 (2023) 102510. https://doi.org/10.1016/j.jcou.2023.102510.
[35] K. Wang, S. Ceulemans, H. Zhang, I. Tsonev, Y. Zhang, Y. Long, M. Fang, X. Li, J. Yan, A. Bogaerts, Inhibiting recombination to improve the performance of plasma-based CO2 conversion, Chemical Engineering Journal 481 (2024) 148684. https://doi.org/10.1016/j.cej.2024.148684.
[36] V. Vermeiren, A. Bogaerts, Plasma-Based CO_2 Conversion: To Quench or Not to Quench?, J. Phys. Chem. C 124 (2020) 18401–18415. https://doi.org/10.1021/acs.jpcc.0c04257.

[37] E. Delikonstantis, M. Scapinello, V. Singh, H. Poelman, C. Montesano, L.M. Martini, P. Tosi, G.B. Marin, K.M. Van Geem, V.V. Galvita, G.D. Stefanidis, Exceeding Equilibrium CO_2 Conversion by Plasma-Assisted Chemical Looping, ACS Energy Lett. 7 (2022) 1896–1902. https://doi.org/10.1021/acsenergylett.2c00632.
[38] Y. Long, X. Wang, H. Zhang, K. Wang, W.-L. Ong, A. Bogaerts, K. Li, C. Lu, X. Li, J. Yan, X. Tu, H. Zhang, Plasma Chemical Looping: Unlocking High-Efficiency CO_2 Conversion to Clean CO at Mild Temperatures, JACS Au 4 (2024) 2462–2473. https://doi.org/10.1021/jacsau.4c00153.
[39] J. Huang, H. Zhang, Q. Tan, L. Li, R. Xu, Z. Xu, X. Li, Enhanced conversion of CO2 into O2-free fuel gas via the Boudouard reaction with biochar in an atmospheric plasmatron, Journal of CO2 Utilization 45 (2021) 101429. https://doi.org/10.1016/j.jcou.2020.101429.
[40] H. Zhang, Q. Tan, Q. Huang, K. Wang, X. Tu, X. Zhao, C. Wu, J. Yan, X. Li, Boosting the Conversion of CO_2 with Biochar to Clean CO in an Atmospheric Plasmatron: A Synergy of Plasma Chemistry and Thermochemistry, ACS Sustainable Chem. Eng. 10 (2022) 7712–7725. https://doi.org/10.1021/acssuschemeng.2c01778.
[41] F. Girard-Sahun, O. Biondo, G. Trenchev, G. Van Rooij, A. Bogaerts, Carbon bed post-plasma to enhance the CO2 conversion and remove O2 from the product stream, Chemical Engineering Journal 442 (2022) 136268. https://doi.org/10.1016/j.cej.2022.136268.
[42] R. Aerts, R. Snoeckx, A. Bogaerts, In-Situ Chemical Trapping of Oxygen in the Splitting of Carbon Dioxide by Plasma: In-Situ Chemical Trapping of O_2 in CO_2 Splitting by DBD, Plasma Process. Polym. 11 (2014) 985–992. https://doi.org/10.1002/ppap.201400091.
[43] J. Wang, K. Zhang, M. Mertens, A. Bogaerts, V. Meynen, Plasma-based dry reforming of methane in a dielectric barrier discharge reactor: Importance of uniform (sub)micron packings/catalysts to enhance the performance, Applied Catalysis B: Environmental 337 (2023) 122977. https://doi.org/10.1016/j.apcatb.2023.122977.
[44] H. Sugiyama, M. Miyazaki, M. Sasase, M. Kitano, H. Hosono, Room-Temperature CO_2 Hydrogenation to Methanol over Air-Stable hcp-PdMo Intermetallic Catalyst, J. Am. Chem. Soc. 145 (2023) 9410–9416. https://doi.org/10.1021/jacs.2c13801.
[45] J.S. Cha, S.H. Park, S.-C. Jung, C. Ryu, J.-K. Jeon, M.-C. Shin, Y.-K. Park, Production and utilization of biochar: A review, Journal of Industrial and Engineering Chemistry 40 (2016) 1–15. https://doi.org/10.1016/j.jiec.2016.06.002.
[46] S. Jung, Y.-K. Park, E.E. Kwon, Strategic use of biochar for CO2 capture and sequestration, Journal of CO2 Utilization 32 (2019) 128–139. https://doi.org/10.1016/j.jcou.2019.04.012.
[47] J. Kopyscinski, R. Habibi, C.A. Mims, J.M. Hill, K_2CO_3 -Catalyzed CO_2 Gasification of Ash-Free Coal: Kinetic Study, Energy Fuels 27 (2013) 4875–4883. https://doi.org/10.1021/ef400552q.
[48] P. Lahijani, Z.A. Zainal, M. Mohammadi, A.R. Mohamed, Conversion of the greenhouse gas CO2 to the fuel gas CO via the Boudouard reaction: A review, Renewable and Sustainable Energy Reviews 41 (2015) 615–632. https://doi.org/10.1016/j.rser.2014.08.034.
[49] R. Roncancio, J.P. Gore, CO2 char gasification: A systematic review from 2014 to 2020, Energy Conversion and Management: X 10 (2021) 100060. https://doi.org/10.1016/j.ecmx.2020.100060.
[50] A. Montoya, T.-T.T. Truong, F. Mondragón, T.N. Truong, CO Desorption from Oxygen Species on Carbonaceous Surface: 1. Effects of the Local Structure of the Active Site and the Surface Coverage, J. Phys. Chem. A 105 (2001) 6757–6764. https://doi.org/10.1021/jp010572l.
[51] C. Ellison, V. Abdelsayed, M. Smith, D. Shekhawat, Comparative evaluation of microwave and conventional gasification of different coal types: Experimental reaction studies, Fuel 321 (2022) 124055. https://doi.org/10.1016/j.fuel.2022.124055.
[52] N. Piatkowski, C. Wieckert, A.W. Weimer, A. Steinfeld, Solar-driven gasification of carbonaceous feedstock—a review, Energy Environ. Sci. 4 (2011) 73–82. https://doi.org/10.1039/C0EE00312C.
[53] N. Gokon, R. Ono, T. Hatamachi, L. Liuyun, H.-J. Kim, T. Kodama, CO2 gasification of coal cokes using internally circulating fluidized bed reactor by concentrated Xe-light irradiation for solar gasification, International Journal of Hydrogen Energy 37 (2012) 12128–12137. https://doi.org/10.1016/j.ijhydene.2012.05.133.
[54] C.J. Viasus Pérez, J.M. Restrepo-Florez, J. Ye, N.T. Nguyen, A.A. Tountas, R. Song, C. Mao, A. Wang, A. Gouda, S. Corapi, S. Ji, H. MacLeod, J. Wu, A. Aspuru-Guzik, C.T. Maravelias, G.A. Ozin, Carbon photochemistry: towards a solar reverse boudouard refinery, Energy Environ. Sci. 16 (2023) 6155–6167. https://doi.org/10.1039/D2EE03353D.
[55] J.A. Menéndez, A. Domínguez, Y. Fernández, J.J. Pis, Evidence of Self-Gasification during the Microwave-Induced Pyrolysis of Coffee Hulls, Energy Fuels 21 (2007) 373–378. https://doi.org/10.1021/ef060331i.

[56] J. Hunt, A. Ferrari, A. Lita, M. Crosswhite, B. Ashley, A.E. Stiegman, Microwave-Specific Enhancement of the Carbon–Carbon Dioxide (Boudouard) Reaction, J. Phys. Chem. C 117 (2013) 26871–26880. https://doi.org/10.1021/jp4076965.
[57] H. Dai, H. Zhao, S. Chen, B. Jiang, A Microwave-Assisted Boudouard Reaction: A Highly Effective Reduction of the Greenhouse Gas CO2 to Useful CO Feedstock with Semi-Coke, Molecules 26 (2021) 1507. https://doi.org/10.3390/molecules26061507.
[58] J.M. Bermúdez, E. Ruisánchez, A. Arenillas, A.H. Moreno, J.A. Menéndez, New concept for energy storage: Microwave-induced carbon gasification with CO2, Energy Conversion and Management 78 (2014) 559–564. https://doi.org/10.1016/j.enconman.2013.11.021.
[59] H.S. Uhm, H.S. Kwak, Y.C. Hong, Carbon dioxide elimination and regeneration of resources in a microwave plasma torch, Environmental Pollution 211 (2016) 191–197. https://doi.org/10.1016/j.envpol.2015.12.053.
[60] P. Liu, X. Liu, J. Shen, Y. Yin, T. Yang, Q. Huang, D. Auerbach, A.W. Kleiyn, CO_2 conversion by thermal plasma with carbon as reducing agent: high CO yield and energy efficiency, Plasma Sci. Technol. 21 (2019) 012001. https://doi.org/10.1088/2058-6272/aadf30.
[61] Z. Li, T. Yang, S. Yuan, Y. Yin, E.J. Devid, Q. Huang, D. Auerbach, A.W. Kleyn, Boudouard reaction driven by thermal plasma for efficient CO2 conversion and energy storage, Journal of Energy Chemistry 45 (2020) 128–134. https://doi.org/10.1016/j.jechem.2019.10.007.
[62] Y. Wu, S.-Z. Li, Y.-L. Niu, H.-J. Yan, D. Yang, J. Zhang, Experimental investigation of CO_2 conversion in Boudouard reaction driven by an atmospheric-pressure microwave plasma torch, J. Phys. D: Appl. Phys. 56 (2023) 065201. https://doi.org/10.1088/1361-6463/acaeda.
[63] A. Luna-Triguero, J.M. Vicent-Luna, M.J. Jansman, G. Zafeiropoulos, M.N. Tsampas, M.C.M. Van De Sanden, H.N. Akse, S. Calero, Enhancing separation efficiency in European syngas industry by using zeolites, Catalysis Today 362 (2021) 113–121. https://doi.org/10.1016/j.cattod.2020.03.061.
[64] C. O'Modhrain, Y. Gorbanev, A. Bogaerts, Post-plasma carbon bed design for CO2 conversion: Does size and insulation matter?, Journal of Energy Chemistry 104 (2025) 312–323. https://doi.org/10.1016/j.jechem.2024.12.066.
[65] N.M. Laurendeau, Heterogeneous kinetics of coal char gasification and combustion, Progress in Energy and Combustion Science 4 (1978) 221–270. https://doi.org/10.1016/0360-1285(78)90008-4.
[66] L.R. Radovic, Active Sites in Graphene and the Mechanism of CO_2 Formation in Carbon Oxidation, J. Am. Chem. Soc. 131 (2009) 17166–17175. https://doi.org/10.1021/ja904731q.
[67] J.-L. Liu, H.-W. Park, W.-J. Chung, D.-W. Park, High-Efficient Conversion of CO2 in AC-Pulsed Tornado Gliding Arc Plasma, Plasma Chem Plasma Process 36 (2016) 437–449. https://doi.org/10.1007/s11090-015-9649-2.
[68] L. Li, H. Zhang, X. Li, X. Kong, R. Xu, K. Tay, X. Tu, Plasma-assisted CO2 conversion in a gliding arc discharge: Improving performance by optimizing the reactor design, Journal of CO2 Utilization 29 (2019) 296–303. https://doi.org/10.1016/j.jcou.2018.12.019.
[69] J. Osorio-Tejada, M. Escriba-Gelonch, R. Vertongen, A. Bogaerts, V. Hessel, CO_2 conversion to CO *via* plasma and electrolysis: a techno-economic and energy cost analysis, Energy Environ. Sci. (2024) 10.1039.D4EE00164H. https://doi.org/10.1039/D4EE00164H.
[70] M. Escribà-Gelonch, J. Osorio-Tejada, R. Vertongen, A. Bogaerts, V. Hessel, Sustainability assessment of plasma-based and electrolytic CO2 conversion to CO, Journal of Cleaner Production (2024) 144578. https://doi.org/10.1016/j.jclepro.2024.144578.
[71] D-CRBN, (2022). https://d-crbn.com/ (accessed December 23, 2024).
[72] T. Nozaki, X. Chen, D.-Y. Kim, H.-H. Kim, Plasma fluidized beds and their scalability, Current Opinion in Green and Sustainable Chemistry 51 (2025) 100984. https://doi.org/10.1016/j.cogsc.2024.100984.
[73] B. Wanten, R. Vertongen, R. De Meyer, A. Bogaerts, Plasma-based CO2 conversion: How to correctly analyze the performance?, Journal of Energy Chemistry 86 (2023) 180–196. https://doi.org/10.1016/j.jechem.2023.07.005.
[74] C.E. Brewer, K. Schmidt-Rohr, J.A. Satrio, R.C. Brown, Characterization of biochar from fast pyrolysis and gasification systems, Env Prog and Sustain Energy 28 (2009) 386–396. https://doi.org/10.1002/ep.10378.
[75] P. Shrestha, D.D. Chun, K. Kang, A.E. Simson, N.B. Klinghoffer, Role of Metals in Biochar Production and Utilization in Catalytic Applications: A Review, Waste Biomass Valor 13 (2022) 797–822. https://doi.org/10.1007/s12649-021-01519-6.
[76] L.L. Alves, A. Bogaerts, V. Guerra, M.M. Turner, Foundations of modelling of nonequilibrium low-temperature plasmas, Plasma Sources Sci. Technol. 27 (2018) 023002. https://doi.org/10.1088/1361-6595/aaa86d.

[77] B. McEnaney, Active Sites in Relation to Gasification of Coal Chars, in: J. Lahaye, P. Ehrburger (Eds.), Fundamental Issues in Control of Carbon Gasification Reactivity, Springer Netherlands, Dordrecht, 1991: pp. 175–203. https://doi.org/10.1007/978-94-011-3310-4_10.
[78] J.M. Calo, M.T. Perkins, A heterogeneous surface model for the “steady-state” kinetics of the boudouard reaction, Carbon 25 (1987) 395–407. https://doi.org/10.1016/0008-6223(87)90011-X.
[79] A. Vimont, F. Thibault-Starzyk, M. Daturi, Analysing and understanding the active site by IR spectroscopy, Chem. Soc. Rev. 39 (2010) 4928. https://doi.org/10.1039/b919543m.
[80] C. Zhang, L. Wu, R. Kang, F. Bin, B. Dou, Precise in-situ infrared spectra and kinetic analysis of gasification under the H2O or CO2 atmospheres, International Journal of Hydrogen Energy 52 (2024) 46–57. https://doi.org/10.1016/j.ijhydene.2023.01.241.
[81] V. Morón, P. Gamallo, R. Sayós, DFT and kinetics study of O/O2 mixtures reacting over a graphite (0001) basal surface, Theor Chem Acc 128 (2011) 683–694. https://doi.org/10.1007/s00214-010-0798-3.
[82] S. Pancheshnyi, B. Eismann, G.J.M. Hagelaar, L.C. Pitchford, ZDPlasKin, (2008). http://www.zdplaskin.laplace.univ-tlse.fr.
[83] K.L. Yang, R.T. Yang, Absolute rates of the carbon-carbon dioxide reaction, AIChE Journal 31 (1985) 1313–1321. https://doi.org/10.1002/aic.690310810.
[84] K.S. Prata, T.E. Schwartzentruber, T.K. Minton, Air–Carbon Ablation Model for Hypersonic Flight from Molecular-Beam Data, AIAA Journal 60 (2022) 627–640. https://doi.org/10.2514/1.J060516.
[85] F. Panerai, T. Cochell, A. Martin, J.D. White, Experimental measurements of the high-temperature oxidation of carbon fibers, International Journal of Heat and Mass Transfer 136 (2019) 972–986. https://doi.org/10.1016/j.ijheatmasstransfer.2019.03.018.
[86] J. Heil, Study and Analysis of Carbon Fiber Recycling., (2011).
[87] A. Lopez-Urionabarrenechea, N. Gastelu, E. Acha, B.M. Caballero, A. Orue, A. Jiménez-Suárez, S.G. Prolongo, I. De Marco, Reclamation of carbon fibers and added-value gases in a pyrolysis-based composites recycling process, Journal of Cleaner Production 273 (2020) 123173. https://doi.org/10.1016/j.jclepro.2020.123173.
[88] I.M.K. Ismail, Structure and active surface area of carbon fibers, Carbon 25 (1987) 653–662. https://doi.org/10.1016/0008-6223(87)90219-3.
[89] C. Qian, Q. Li, Z. Zhang, X. Wang, J. Hu, W. Cao, Prediction of higher heating values of biochar from proximate and ultimate analysis, Fuel 265 (2020) 116925. https://doi.org/10.1016/j.fuel.2019.116925.
[90] L. Leng, Q. Xiong, L. Yang, H. Li, Y. Zhou, W. Zhang, S. Jiang, H. Li, H. Huang, An overview on engineering the surface area and porosity of biochar, Science of The Total Environment 763 (2021) 144204. https://doi.org/10.1016/j.scitotenv.2020.144204.
[91] L.R. Radović, P.L. Walker, R.G. Jenkins, Importance of carbon active sites in the gasification of coal chars, Fuel 62 (1983) 849–856. https://doi.org/10.1016/0016-2361(83)90041-8.
[92] K. Xu, S. Hu, S. Su, C. Xu, L. Sun, C. Shuai, L. Jiang, J. Xiang, Study on Char Surface Active Sites and Their Relationship to Gasification Reactivity, Energy Fuels 27 (2013) 118–125. https://doi.org/10.1021/ef301455x.
[93] R.O. Lussow, F.J. Vastola, P.L. Walker, Kinetics of oxygen interaction with graphon between 450 and 675°C, Carbon 5 (1967) 591–602. https://doi.org/10.1016/0008-6223(67)90039-5.
[94] S. Ahmed, M.H. Back, J.M. Roscoe, A kinetic model for the low temperature oxidation of carbon: I, Combustion and Flame 70 (1987) 1–16. https://doi.org/10.1016/0010-2180(87)90155-6.
[95] L.R. Radovic, Chemistry & Physics of Carbon: Volume 30, CRC Press, 2007. https://books.google.be/books?id=4_aML88vmh8C.
[96] J. Slaets, B. Loenders, A. Bogaerts, Plasma-based dry reforming of CH4: Plasma effects vs. thermal conversion, Fuel 360 (2024) 130650. https://doi.org/10.1016/j.fuel.2023.130650.
[97] G. Trenchev, St. Kolev, W. Wang, M. Ramakers, A. Bogaerts, CO_2 Conversion in a Gliding Arc Plasmatron: Multidimensional Modeling for Improved Efficiency, J. Phys. Chem. C 121 (2017) 24470–24479. https://doi.org/10.1021/acs.jpcc.7b08511.
[98] W. Xu, S. Van Alphen, V.V. Galvita, V. Meynen, A. Bogaerts, Effect of Gas Composition on Temperature and CO_2 Conversion in a Gliding Arc Plasmatron reactor: Insights for Post-Plasma Catalysis from Experiments and Computation, ChemSusChem 17 (2024) e202400169. https://doi.org/10.1002/cssc.202400169.
[99] A. Salden, M. Budde, C.A. Garcia-Soto, O. Biondo, J. Barauna, M. Faedda, B. Musig, C. Fromentin, M. Nguyen-Quang, H. Philpott, G. Hasrack, D. Aceto, Y. Cai, F.A. Jury, A. Bogaerts, P. Da Costa, R. Engeln, M.E. Gálvez, T. Gans, T. Garcia, V. Guerra, C. Henriques, M. Motak, M.V. Navarro, V.I. Parvulescu, G. Van Rooij, B. Samojeden, A. Sobota, P. Tosi, X.

Tu, O. Guaitella, Meta-analysis of CO2 conversion, energy efficiency, and other performance data of plasma-catalysis reactors with the open access PIONEER database, Journal of Energy Chemistry 86 (2023) 318–342. https://doi.org/10.1016/j.jechem.2023.07.022.